Interference-Based QoS and Capacity Analysis of VANETs for Safety Applications

Jing Zhao, *Member, IEEE*, Yanbin Wang, HuaLin Lu, Zhijuan Li, and Xiaomin Ma, *Senior Member, IEEE*

***Abstract*— Whether the current IEEE 802.11p communication system meets the stringent quality of service (QoS) requirements for safety applications or not is still not very clear. Signal-to-interference-plus-noise ratio (SINR) distribution plays a primary role in quantifying the QoS as well as link capacity of IEEE 802.11p in one-dimensional (1-D) highway and two-dimensional (2-D) intersection road. Most of the analytical models based on stochastic geometry assumed ALOHA access to analyze the SINR distribution, while few of the works developed the stochastic geometry based model considering CSMA access but derived the SINR distribution utilizing statistical estimator. On the other hand, the current interference based probability analytic model for the SINR distribution limit the 1-D extension to 2-D, due to the very high numerical computational complexity at 2-D. In this paper, we propose an analytic model under more general non-homogeneous Poisson process (NHPP) node distribution, more general channel fading model (*Nakagami*) with path loss, and noise, for the study of QoS and capacity of VANET for BSM based safety applications in both 1-D highway and 2-D intersection road. The proposed model derives QoS and capacity of VANET BSM broadcast through evaluation of SINR distribution using probability theory and ordered statistics, which has much lower computational complexity compared with the unordered statistic model. The proposed model is validated by NS2 simulation and extended to the derivation of other QoS metrics such as packet reception probability, packet reception ratio, and broadcast link capacity, etc. The performance comparisons between 1-D and 2-D are implemented, and the QoS sensitivity analyses regarding the extension to multi-intersection as well as enlarging interference range are discussed.**

***Index Terms*—Capacity, quality of service, safety applications, signal-to-interference-plus-noise ratio, vehicular ad hoc networks.**

Manuscript received March 27, 2020; revised August 24, 2020 and January 23, 2021; accepted February 11, 2021. Date of publication February 16, 2021; date of current version April 2, 2021. This work was supported in part by the National Nature Science Foundation of China under Grant 61 572 150, in part by the Fundamental Research Funds for the Central Universities of DUT, under Grant DUT17RC(3)097, and in part by the Key Research and Development Program of Guangdong Province under Grant 2019B010136003. The review of this article was coordinated by Prof. Chadi Assi. *(Corresponding author: jing zhao.)*

Jing Zhao is with the School of Software, Dalian University of Technology, DaLian, Liaoning 116024, China (e-mail: zhaoj9988@dlut.edu.cn).

Yanbin Wang is with the Department of Industrial Engineering, Harbin Institute of Technology, 150001 Harbin, China (e-mail: wangyb@hit.edu.cn).

HuaLin Lu and Zhijuan Li are with the Department of Computer Science, and Technology, Harbin Engineering University, 150001 Harbin, China (e-mail: n.betula.lu@gmail.com; lizhijuan@hrbeu.edu.cn).

Xiaomin Ma is with the College of Science, and Engineering, Oral Roberts University, Tulsa, OK 74171 USA (e-mail: xma@oru.edu).

Digital Object Identifier 10.1109/TVT.2021.3059740

I. Introduction

A. Motivation

VEHICLE to vehicle (V2V) safety communication based on dedicated short range communication (DSRC) radio technology [1][2] at 5.9 GHz band allocated 10 MHz channels, is projected to support low-latency and reliable wireless data communications to enable collision prevention safety applications for intelligent transportation system (ITS) [3]. The main safety operation for DSRC is to transmit two types of safety messages: basic safety messages (BSMs, also known as a beacon) or event-driven safety messages (ESMs). BSMs, which are periodic, convey information about the state of the vehicles (e.g., position, speed, direction, *etc.*). Event-driven safety messages, or ESMs, which are bursty, contain information about emergencies (e.g., sudden hard braking, intersection collision warning, approaching ambulance warning, *etc.*) and environmental hazards. DSRC system based VANETs use one-hop or multi-hop broadcasting to disseminate real-time traffic information or safety-related messages [4], [5]. Among 75 safety-related application scenarios identified [6], [7], performance analyses of the typical one-dimensional (1-D) and two-dimensional (2-D) intersection VANET safety applications have been recognized to be critical and common situations for V2V communications. IEEE 802.11p as PHY as well as MAC layer standard for DSRC has been implemented to accommodate V2V communications for safety applications. The performance of IEEE 802.11p is affected by several factors such as vehicle location, vehicle density, channel condition, and network geometry, *etc.* [8]. Prior studies have shown that IEEE 802.11p performance will degrade at high density, and the reliability metric requirements do not be guaranteed at the typical 1-D and 2-D intersection scenarios [9], [10] [11].

SINR distribution plays an important role in quantifying the QoS as well as the link capacity of VANETs. The main mathematical tools are stochastic geometry theory and probability modeling. Most of the stochastic geometry and point processes based models could be used to model the ALOHA access since the analytical tractable for ALOHA [12][13] [14]. Few of the works use stochastic geometry to model the CSMA based MAC protocol. Authors in [15] utilized ALOHA to approximate the CSMA MAC protocol to analyze the dense vehicular network. The work presented in [10] concentrated on combining queueing theory and modified Matérn hard-core process to characterize the CSMA backoff process capturing the concurrent transmission. However, the model could not derive the SINR distribution analytically, and the obtaining statistical values of SINR still rely heavily on the statistical parameter values through simulation. Ni *et al.* [16] and Ma *et al.* [17] assumed lognormal vehicle distribution, and obtained the SINR distribution through interference distance distribution as well as interference power distribution. However, the complex numerical integral operations of SINR distribution make the computation load very high, as a result, the modeling technique in 1-D as well as vehicle lognormal distribution assumption could not be extended to the 2-D intersection to analyze the SINR distribution.

We properly model the interference distance distribution accounting for the distance distribution of transmitter to interferers, and the distance between transmitter to receivers, of 1-D as well as 2-D intersection road by the ordered statistic. The reasonable assumptions regarding vehicle NHPP distribution, the *Nakagami* fading channel, and noise effect are concentrated in the proposed model. The interference distance distribution is firstly deduced with the help of the ordered statistic and later the accumulated power distribution at the receiver is obtained, thus the SINR, as well as link capacity distribution, is derived analytically. Simulations in NS2 incorporating SUMO (Microscopic traffic simulation) mobility vehicle [18], are implemented to verify the effectiveness and accuracy of our proposed model.

B. Related Work

A lot of analytical models along with extensive simulations have been proposed to study the performance and the reliability of DSRC IEEE 802.11p broadcast services in 1-D highway VANET as well as 2-D intersection. The simulation model is time-consuming to test the combination of system parameters, while the analytical model could characterize the realistic traffic situations to reduce computation load, and give insightful optimization schemes to enhance the capability of DSRC. There are mainly divided into two kinds of modeling techniques: deterministic communication range based and interference based.

Most deterministic communication range based analytical models for 1-D are [19] [20][21] [22][8], others for 2-D VANETs at intersections are [23][24]. Deterministic analytical models assume deterministic communication range, taking account of the hidden terminal, *Nakagami* fading model or *Rayleigh* fading channel model, and point-to-point packet reception probability (PRP) and packet reception ratio (PRR) are reliability metrics used to evaluate IEEE 802.11p. However, the deterministic communication range assumptions are not practical, moreover, many unpractical assumptions such as exponential vehicle distributions, and *Rayleigh* fading channel model with path loss, *etc*. are made for tractability of the analytical models. Besides, it also could not quantify the VANET performance metric link capacity to be used for evaluating the actual performance of a link or the entire VANETs.

Interference based models mainly employ the stochastic geometry and probability approach to characterize the behavior of IEEE 802.11p, while the reliability evaluations depend on SINR distribution numerical solutions. Stochastic geometry approaches [25] consider the vehicle location, road geometry, and interference geometry, assume that the interference vehicle nodes follow the PPP and utilize the Matérn core process to obtain the SINR distribution statistically. Several models based on the stochastic geometry approach were reported for performance analysis of safety applications regarding V2V in 1-D VANETs [26][10] [15][27] [28] and 2-D VANETs at intersections [14][29] [12][13] [30]. Besides, [31] [32] [33], focused on modeling cellular vehicle-to-everything (C-V2X) utilizing the sophisticated Poisson line Cox process, to give the related QoS metrics such as the coverage probability, rate coverage, *etc*. [31] proposed a novel heterogeneous cellular network with both planar and vehicle base stations to analyze the coverage probability perceived by typical users on roads. The analyses concentrated on the snapshot of the network using palm probability, and the *Rayleigh* fading channel, distance-based path loss, and noise power is negligible in the transmission model. [32] analyzed the downlink SIR-based coverage probability and rate coverage of a C-V2X considering the shadowing effect in the spatial model. [33] directly modeled sharing of V2V and cellular uplink frequency for C-V2X and infrastructure mode to improve spectral efficiency. The above works researched the C-V2X framework focusing on the coupling relations for the base station, vehicle node, and cellular downlink or uplink instead of CSMA for 1-D and 2-D cases. So it could not be directly used to analyze the performance of CSMA of V2V communications. Most stochastic geometry based models assumed ALOHA channel access, Poisson node distribution, and *Rayleigh* channel fading model [12] [14][29] [27][28] [30]. In [12], the success probabilities for 1-D and 2-D intersection users are analyzed. [30] focused on the reliability of V2V under line of sight and non-line-of-sight scenarios. [14] presented an analytic model for the spatial case accounting for the clustering effect of vehicles at an intersection, where the transmitter probability and the distance between the receiver and transmitter are utilized to capture the clustering effect. Authors in [29] developed a general framework for accident-prone intersection scenarios to analyze the packet reception probability, and simply considered the ALOHA case obtaining the numerical SINR distribution. [27] [28] focused on investigating how the urban structure affects the roadside unit (RSU) placement or V2V communication at the intersection, and authors in [27] focused on obtaining the optimal transmission range control, achieving performance gain. However, the above mentioned resulting models are just applicable to ALOHA channel access and *Rayleigh* fading due to analytically tractable, while suitable different 1-D or 2-D scenarios. [15] [13] used ALOHA to approximate the CSMA under the high density of VANET, and the closed-form analytical expressions for outage probability are investigated in [13]. [10] assumed CSMA channel access, Poisson node distribution, and *Rayleigh* channel fading model, taking account of noise effect. However, it did not obtain the closed-form analytical expressions for the SINR distribution, instead of utilizing the hard-core process to obtain the SINR distribution statistically under the spatial, intermediate, and high density. Ni *et al.* and Ma *et al.* [16][17] did not consider the noise effect applied for the proposed probability model for the 1-D scenario, whereas computational complexity for computing SINR distribution is so high that it does not adapt to analyze the QoS and capacity at an actual case. The above mentioned researches analyzed the QoS metric like outage probability similar to the meaning of PRP, but they did not analyze the link capacity except for Ni *et al.* and Ma *et al.* [16][17].

C. Our Proposed Model and Challenges

We proposed the analytical model taking account of *Nakagami* fading, vehicle NHPP distribution, and noise effect for 1-D as well as 2-D intersections. We consider the vehicle node following NHPP to characterize the real traffic situations as well as the effect of traffic lights [24][34]. There may exist combinations for both the number of interference areas in 1-D as well as 2-D and whether the interference vehicle node is transmitting in each area, and the occurrence probability of each combination could be derived according to the probability of a vehicle at transmitting state for the analytical model [8]. The interference distance distribution could be further obtained with the total probability, which consists of interference node transmitting as well as noise effect. Thus, the SINR distribution and then link capacity distribution could be analytically solved. The parameters for transmission range, carrier sensing range, and interference range are set reasonably according to reference in [35][16]. Our proposed model enables the evaluation of QoS metrics as well as VANET capacity for safety applications in a more practical and effective way, by taking account of road geometry (1-D and 2-D) under basis on probability modeling instead of stochastic geometry approach. Our proposed analytical model could be used to make decisions of the network design, as well as adaptive schemes to tune communication network parameters for the best QoS depending on the available link capacity [36][11].

There are mainly three challenges overcoming to derive the cumulative distribution function (CDF) of SINR. The first challenge here is to make the analytical CDF of SINR have numerical solutions and less computation load. However, only in 1-D highway with lognormal node distribution scenario the big computation load from numerical integrations limit extensive usage of the model in the design and plan of VANETs for safety applications [16][17]. We introduce the order statistics $f_{D_{\mathrm{S}}}$ (the distance distribution between the sending node and receiving node) and $f_{D_i}(i = I_1, I_2, I_3, I_4$, the distance distribution between the interference node and receiving node), to reduce the computational complexity of SINR distribution. Thanks to the NHPP node distribution, the formula is greatly simplified. The computational complexity of [16], [17] with the introducing order statistics could be reduced by $O(n)$ times and becomes constant. In the same way, the computational complexity of 1-D highway and 2-D intersection can be reduced by $O(n^2)$ and $O(n^4)$ times, respectively. Here, the "n" is the upper limit of the number of vehicles in the range of communication.

The second challenge here is to cross-validate our proposed model with the NS2 simulation results. In NS2, Chen *et al.* [37], [38] designed and developed the revised modules for the IEEE 802.11 protocol, which are widely used in the simulation of VANETs by researchers. The modified version adopts the SINR based method to determine whether an incoming signal is received or not. However, the SINR thresholds (SINRTs) are fixed values in terms of the modulation schemes and corresponding data rates. Li *et al.* [38] has already pointed out the inflexible SINRT settings, and thus we further modified the NS2 source code and compiled it to make it adapt to the SINRT settings by the user's requirement in the simulation.

The third challenge here is to give the computational complexity of CDF of SINR comparisons between the model with order statistics and unordered statistics, and thus validate our proposed model effectiveness. The Monte Carlo as well as the Message Passing Interface (MPI) method [39] is utilized to compute the SINR distribution with an unordered statistical model since VANET QoS numerical solutions need a lot of time to compute.

D. Contribution

The main contributions of this paper are summarized as follows:

- An analytic model based on SINR is built with NHPP node distribution in both 1-D highway and 2-D intersection, by taking account of CSMA access, *Nakagami* channel fading with path loss, noise effect, and impact of the hidden terminals and concurrent transmissions;
- The proposed model derives the closed-form analytical expressions of SINR distribution through a new approach of NHPP ordered statistics, which reduces the computational complexity of the derivation significantly;
- The Monte Carlo, as well as MPI method, is utilized to calculate for the unordered statistical model, and the experimental results give the computational complexity comparisons between the model with order statistics and unordered statistics;
- QoS metrics and capacity metrics such as link capacity are defined and evaluated;
- We devise the new $WirelessPhy$ class to make the NS2 simulation adapt to flexible SINRT settings.

E. Organization

The rest of the paper is organized as follows: Section II presents an analytical model for 1-D VANETs and assumptions for NHPP node distribution, noise effect, and *Nakagami* channel fading with path loss, under which the analytic model is built. The QoS reliability, as well as capacity metrics in 1-D, are obtained. Section III presents an analytical model for 2-D VANETs, assuming that the interferences are within the right, left on the X-axis, up, and down on the Y-axis. An approach of NHPP ordered statistics is also proposed to reduce the computational complexity of CDF of SINR. Accordingly, the QoS and capacity metrics for 2-D are obtained. Section IV modify the source code of wireless module in NS2 to achieve flexible setting of SINRTs, present the parameter setting with 1-D and 2-D scenarios where the positions of vehicles follow NHPP, and compare the performance of the static scene simulation and mobility scene simulation based on the traffic generated by SUMO and NS2 build-in mobility model. Section V gives the computation efficiency comparisons between the order statistic model and unordered, presents the comparison results between the numerical and simulation, analyzes the performance difference between 1-D and 2-D scenes and then gives the probability density function (PDF) of the link capacity of different VANET scenes. Section VI further obtain the PRR considering multiple intersections beyond the carrier sensing range. The paper is concluded in Section VII.

II. QoS and Capacity of Beacon Message Broadcast in One-Dimensional VANETs

In this section, we first give the assumptions, secondly analyze the solution steps for the derivation of CDF of SINR, which require solving interference location distribution as inputs to obtain the CDF of SINR. Finally, the CDF as well as PDF of SINR, link capacity could be obtained.

A. Assumptions and Channel Model

We assume that IEEE 802.11p beacon message broadcast works under the following scenarios. (1) A 2-D strip-like network area can be approximated to a 1-D single lane. (2) All vehicles are equipped with DSRC communication capability. (3) All nodes are treated as homogeneous with identical vehicle length $L_{\rm V}$ and transmission power $P_{\rm t}$. (4) Mobile nodes are placed on the lines according to NHPP with the density of vehicles at a distance x from the tagged node: $\beta(x)$ (in nodes per meter). Then the probability of finding i vehicles in a space interval $(x, x+l)$ is given by

$$P[i,(x,x+l)] = \frac{\left(\int_x^{x+l}\beta(z)\mathrm{d}z\right)^i \exp\left(-\int_x^{x+l}\beta(z)\mathrm{d}z\right)}{i!}.$$

(5) Channel fading effect: *Nakagami* fading model. (6) According to [35] and [16], the distance between an interferer and the tagged transmitter should be no longer than $2r_{\rm E}$, which has been confirmed to be quite accurate. $r_{\rm E}$ is the average sensing range $r_{\rm E} = d_0\sqrt[\alpha]{P_{\rm t}\eta/P_{\rm th}}$, and $P_{\rm th}$ is the clear channel assessment (CCA) sensitivity.

The PDF of the power $P_{\rm r}$ received at a distance d from the source node is given by

$$f_{P_{\rm r}|d}(x) = \frac{1}{\Gamma(m)}\left(\frac{m}{\bar{P}_{\rm r}(d)}\right)^m x^{m-1}\exp\left(-\frac{mx}{\bar{P}_{\rm r}(d)}\right), \quad (1)$$

where $\Gamma(\cdot)$ is the Gamma function, and m is the fading parameter. $\bar{P}_{\rm r}(d) = P_{\rm t}\eta(\frac{d_0}{d})^\alpha$ (η is a transceiver-determined constant, d_0 is the reference distance for the far-zone field, α is the path loss exponent) is the mean determined by the path loss.

B. Cdf of Sinr

Many studies regard $P(\mathrm{SINR} > \theta) = 1 - P(\mathrm{SINR} \le \theta)$ as an important standard for evaluating the performance of VANETs, and our research also analyzes the derivation of CDF of SINR. $\mathrm{SINR} = P_{\rm r}/(P_{\rm I}+P_{\rm n})$, $P_{\rm r}$ is the power of the received signal, $P_{\rm I}$ is the interference power at the receiver, and $P_{\rm n}$ is the noise power. When there exists interference node transmitting, whereas $P_{\rm I}$ is much larger than $P_{\rm n}$, then SINR could be approximately expressed as $\mathrm{SINR_I} = P_{\rm r}/P_{\rm I}$. Otherwise, SINR can be expressed as $\mathrm{SINR_n} = P_{\rm r}/P_{\rm n}$ denoted as without interferer. Thus, the PDF and CDF of SINR may be derived based on the occurrence probability of $\mathrm{SINR_I}$ and $\mathrm{SINR_n}$, respectively.

The PDF of $\mathrm{SINR_I}$ may be obtained by using the convolution quotient formula of $P_{\rm r}$ as well as $P_{\rm I}$, where (1) gives the PDF of $P_{\rm r}$, while the PDF of $\mathrm{SINR_n}$ may be obtained by PDF of $P_{\rm r}$ assuming that $P_{\rm n}$ is a constant.

From the above analyses, we know that the main problem is to derive PDF of $P_{\rm I}$, where the interference distance distribution should be formulated first and then represented as next.

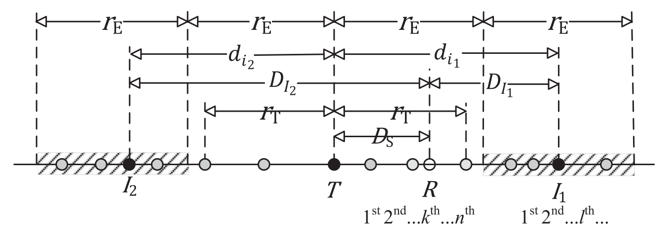

Fig. 1. General interfering scenario for VANET safety message broadcast [16].

C. The Interference Distance Distribution

As shown in Fig. 1 in [16], $r_{\rm E}$ and $r_{\rm T}$ denote the channel sensing range and the transmission range, respectively, where $r_{\rm T} \le r_{\rm E}$ [16]. $D_{\rm S}$ denotes the distance between the source node T and the target node R. $I_1(I_2)$ is the interference node within the right(left) shaded region with distance to T as $[r_{\rm E}, 2r_{\rm E}]$. Assuming that there are $l(l')$ nodes in the right(left) shaded region, $d_{i_1}(i_1 = 1,\ldots,l)(d_{i_2}(i_2 = 1,\ldots,l'))$ denote the distance between the tagged node T and the $i_1(i_2)$-th node within the right(left) shaded region. $D_{I_1}(D_{I_2})$ denotes the distance between the interference node $I_1(I_2)$ and the R, $D_{I_1} + D_{\rm S} = d_{i_1}(D_{I_2} = D_{\rm S} + d_{i_2})$.

Given NHPP distribution of the distance between nodes, and independent random variables $r_{\rm E} \le S_{i_1} \le 2r_{\rm E}$ denoting unordered distances between T and the nodes in the right shaded region. Let the number of vehicles in the interval $[r_{\rm E}, r]$, $[r_{\rm E}, 2r_{\rm E}]$ be denoted by $N(r)$, $N(s)$, respectively. The CDF of S_{i_1} is given by Theorem 6.2 in [40].

$$\begin{aligned} F_{S_{i_1}}(r) &= P(S_{i_1} \le r | N(r_{\rm E}) = 1) \\ &= \frac{P[N(r) = 1, N(s) - N(r) = 0]}{P[N(s) = 1]} \\ &= \frac{\int_{r_{\rm E}}^{r}\beta(z)\mathrm{d}z}{\int_{r_{\rm E}}^{2r_{\rm E}}\beta(z)\mathrm{d}z}, r_{\rm E} \le r \le 2r_{\rm E}, i_1 = 1,\ldots,l. \end{aligned} \quad (2)$$

Then the PDF of S_{i_1} is:

$$f_{S_{i_1}}(r) = \frac{\beta(r)}{\int_{r_{\rm E}}^{2r_{\rm E}}\beta(z)\mathrm{d}z}. \quad (3)$$

Then according to Theorem 6.2 in [40], $d_{i_1}(i_1 = 1,\ldots,l)$ are the order statistics of the random variables $S_{i_1}(i_1 = 1,\ldots,l)$. Thus, the CDF and PDF of distance $d_{i_1}(r_{\rm E} \le d_{i_1} \le 2r_{\rm E})$ can be calculated as

$$F_{d_{i_1}}(\tau)=P(d_{i_1}\leq\tau)=\sum_{j=i_1}^{l}\binom{l}{j}F_{S_{i_1}}^{j}(\tau)\big[1-F_{S_{i_1}}(\tau)\big]^{l-j},$$
$$f_{d_{i_1}}(\tau)=\frac{\mathrm{d}F_{d_{i_1}}(\tau)}{\mathrm{d}\tau},r_{\mathrm{E}}\leq\tau\leq 2r_{\mathrm{E}}. \tag{4}$$

Let $D_{\mathrm{S}}=d_{\mathrm{s}}$, assume that I_1 is the i_1-th node in the right shaded region. The conditional CDF of $D_{I_1}(r_{\mathrm{E}}-D_s\leq D_{I_1}\leq 2r_{\mathrm{E}}-D_s)$ can be defined as

$$\begin{aligned}F_{D_{I_1}|(d_{\mathrm{s}},i_1)}(x)&=P(D_{I_1}\leq x|d_{\mathrm{s}})\\&=P(d_{i_1}-d_{\mathrm{s}}\leq x|d_{\mathrm{s}})\\&=P(d_{i_1}\leq x+d_{\mathrm{s}}|d_{\mathrm{s}})\\&=F_{d_{i_1}}(x+d_{\mathrm{s}}),i_1=1,\ldots,l.\end{aligned} \tag{5}$$

The PDFs of the distances of the individual interfering nodes to the receiver R are obtained as

$$f_{D_{I_1}|(d_{\mathrm{s}},i_1)}(x)=\frac{\mathrm{d}F_{D_{I_1}|(d_{\mathrm{s}},i_1)}(x)}{\mathrm{d}x}=f_{d_{i_1}}(x+d_{\mathrm{s}}). \tag{6}$$

The probability that there are l nodes in the shaded area is

$$P[l,(r_{\mathrm{E}},2r_{\mathrm{E}})]=\frac{\left(\int_{r_{\mathrm{E}}}^{2r_{\mathrm{E}}}\beta(x)\mathrm{d}x\right)^{l}\exp\left(-\int_{r_{\mathrm{E}}}^{2r_{\mathrm{E}}}\beta(x)\mathrm{d}x\right)}{l!}.$$

Then, the D_{I_1}'s conditional PDF can be expressed as

$$f_{D_{I_1}|d_{\mathrm{s}}}(x)=\sum_{l=1}^{\infty}P[l,(r_{\mathrm{E}},2r_{\mathrm{E}})]\sum_{i_1=1}^{l}f_{D_{I_1}|(d_{\mathrm{s}},i_1)}(x)p_{i_1}, \tag{7}$$

where p_{i_1} is the probability that the interferer I_1 is the i_1-th node within the right shaded area, which is evaluated as $p_{i_1}=1/l(i_1=1,\ldots,l)$. Thus, (7) can be expressed as

$$\begin{aligned}f_{D_{I_1}|d_{\mathrm{s}}}(x)&=\sum_{l=1}^{\infty}P[l,(r_{\mathrm{E}},2r_{\mathrm{E}})]\sum_{i_1=1}^{l}f_{d_{i_1}}(x+d_s)\frac{1}{l}\\&=f_{S_{i_1}}(x+d_s)\\&=\frac{\beta(x+d_s)}{\int_{r_{\mathrm{E}}}^{2r_{\mathrm{E}}}\beta(z)\mathrm{d}z}.\end{aligned} \tag{8}$$

Similarly, the CDF and PDF of I_2's interference power at R can also be derived. Independent random variables $S_{i_2}(r_{\mathrm{E}}\leq S_{i_2}\leq 2r_{\mathrm{E}})$ denoting unordered distance between T and the nodes in the left shaded region, the CDF and PDF of S_{i_2} are

$$F_{S_{i_2}}(r)=\frac{\int_{-r}^{-r_{\mathrm{E}}}\beta(z)\mathrm{d}z}{\int_{-2r_{\mathrm{E}}}^{-r_{\mathrm{E}}}\beta(z)\mathrm{d}z},f_{S_{i_2}}(r)=\frac{\beta(-r)}{\int_{-2r_{\mathrm{E}}}^{-r_{\mathrm{E}}}\beta(z)\mathrm{d}z},$$
$$r_{\mathrm{E}}\leq r\leq 2r_{\mathrm{E}},i_2=1,2,\ldots,l'.$$

PDF of D_{I_2} can be obtained based on deduction process from (4) to (8):

$$f_{D_{I_2}|d_{\mathrm{s}}}(x)=\frac{\beta(d_{\mathrm{s}}-x)}{\int_{-2r_{\mathrm{E}}}^{-r_{\mathrm{E}}}\beta(z)\mathrm{d}z}. \tag{9}$$

(8), (9) are the distance distribution of interference nodes, which is briefly formulated with the introduction of order statistics. In this way, the computational complexity becomes constant. Otherwise, the complexity of (13) of 1-D and (29) of 2-D intersection are $O(n^2)$ and $O(n^4)$, respectively. Latter the experiments will show the comparisons of running time for ordered *vs.* unordered case.

D. PDF of SINR With Interference

The CDF and PDF of I_1's interference power P_{I_1} received at R according to (1) and (8) could be presented as

$$\begin{aligned}F_{P_{I_1}|d_{\mathrm{s}}}(x)&=P(P_{I_1}\leq x|D_{\mathrm{S}}=d_{\mathrm{s}})\\&=\int_{t'=0}^{x}\int_{r_{\mathrm{E}}-d_{\mathrm{s}}}^{2r_{\mathrm{E}}-d_{\mathrm{s}}}f_{P_{\mathrm{r}}|D_{I_1}}(t')f_{D_{I_1}|d_{\mathrm{s}}}(t)\mathrm{d}t\mathrm{d}t',\\f_{P_{I_1}|d_{\mathrm{s}}}(x)&=\frac{\mathrm{d}F_{P_{I_1}|d_{\mathrm{s}}}(x)}{\mathrm{d}x}.\end{aligned}$$

The CDF and PDF of I_2's interference power P_{I_2} received at R can be obtained by (1) and (9):

$$\begin{aligned}F_{P_{I_2}|d_{\mathrm{s}}}(x)&=P(P_{I_2}\leq x|D_{\mathrm{S}}=d_{\mathrm{s}})\\&=\int_{t'=0}^{x}\int_{r_{\mathrm{E}}+d_{\mathrm{s}}}^{2r_{\mathrm{E}}+d_{\mathrm{s}}}f_{P_{\mathrm{r}}|D_{I_2}}(t')f_{D_{I_2}|d_{\mathrm{s}}}(t)\mathrm{d}t\mathrm{d}t',\\f_{P_{I_2}|d_{\mathrm{s}}}(x)&=\frac{dF_{P_{I_2}|d_{\mathrm{s}}}(x)}{\mathrm{d}x}.\end{aligned}$$

[8] built a semi-Markov based queueing model to characterize the CSMA/CA backoff mechanism, and obtain the π_{XMT} which is the steady-state probability that a vehicle is in the transmission state. According to π_{XMT}, the probability that a node in the shaded area transmits during the vulnerable period of the transmission from the tagged node T is evaluated as

$$p_t=\pi_{XMT}\frac{2(T_{\mathrm{p}}-\mathrm{DIFS})}{T_{\mathrm{p}}}, \tag{10}$$

where T_{p} is the mean sojourn time in *XMT* state, DIFS is distributed interframe space. Then, the probability that there is interference in the right shaded region is

$$\begin{aligned}p_1&=1-\sum_{i=0}^{\infty}(1-p_{\mathrm{t}})^{i}\frac{(\int_{r_{\mathrm{E}}}^{2r_{\mathrm{E}}}\beta(x)\mathrm{d}x)^{i}}{i!}\exp\left(-\int_{r_{\mathrm{E}}}^{2r_{\mathrm{E}}}\beta(x)\mathrm{d}x\right)\\&=1-\exp\left(-p_{\mathrm{t}}\int_{r_{\mathrm{E}}}^{2r_{\mathrm{E}}}\beta(x)\mathrm{d}x\right),\end{aligned} \tag{11}$$

and the probability that there is interference in the left shaded region is

$$\begin{aligned}p_2&=1-\sum_{i=0}^{\infty}(1-p_{\mathrm{t}})^{i}\frac{(\int_{-2r_{\mathrm{E}}}^{-r_{\mathrm{E}}}\beta(x)\mathrm{d}x)^{i}}{i!}\exp\left(-\int_{-2r_{\mathrm{E}}}^{-r_{\mathrm{E}}}\beta(x)\mathrm{d}x\right)\\&=1-\exp\left(-p_{\mathrm{t}}\int_{-2r_{\mathrm{E}}}^{-r_{\mathrm{E}}}\beta(x)\mathrm{d}x\right).\end{aligned} \tag{12}$$

Three cases need to be considered to get the PDF of SINR with interference:

1) There are interferers in the right shaded region, and no interferers in the left shaded region:
the probability is $p_1(1-p_2)$, the PDF of the interference power is $f_{P_{I_1}|d_s}(x)$.
2) There are interferers in the left shaded region, and no interferers in the right shaded region:
the probability is $p_2(1-p_1)$, the PDF of the interference power is $f_{P_{I_2}|d_s}(x)$.
3) Interferers exist in both the left and right shaded region:
the probability is $p_1 \cdot p_2$, the PDF of the interference power is

$$f_{P_{I_1+I_2}|d_{\mathrm{s}}}(x) = \int_0^{\infty} f_{P_{I_1}|d_{\mathrm{s}}}(x-t) f_{P_{I_2}|d_{\mathrm{s}}}(t)\mathrm{d}t. \quad (13)$$

From the total probability formula, the PDF of the total interference power P_{I} accumulated at the receiver R is denoted as

$$\begin{aligned} f_{P_{\mathrm{I}}|d_{\mathrm{s}}}(x) &= p_1(1-p_2) f_{P_{I_1}|d_{\mathrm{s}}}(x) \\ &\quad + p_2(1-p_1) f_{P_{I_2}|d_{\mathrm{s}}}(x) \\ &\quad + p_1 p_2 f_{P_{I_1+I_2}|d_{\mathrm{s}}}(x), f_{\mathrm{SINR_I}|(d_{\mathrm{s}},P_{\mathrm{r}}>P_{\mathrm{th}})}(x) \\ &= \int_{\mathrm{Max}\{\frac{P_{\mathrm{th}}}{x},P_{\mathrm{th}}\}}^{\infty} t \cdot f_{P_{\mathrm{r}}|d_{\mathrm{s}}}(t\cdot x) f_{P_{\mathrm{I}}|d_{\mathrm{s}}}(t)\mathrm{d}t. \end{aligned} \quad (14)$$

E. PDF of SINR Without Interference

The probability that there are no interferers in both the left and right shaded region is $(1-p_1)\cdot(1-p_2)$, the noise power is assumed to be constant with the value of P_{n}, $\mathrm{SINR_n} = P_{\mathrm{r}}/P_{\mathrm{n}}$.

$$\begin{aligned} &F_{\mathrm{SINR_n}|(d_{\mathrm{s}},P_{\mathrm{r}}>P_{\mathrm{th}})}(x) \\ &= (1-p_1)(1-p_2)P(\mathrm{SINR_n} \le x | P_{\mathrm{r}} > P_{\mathrm{th}}) \\ &= (1-p_1)(1-p_2)P\left(\frac{P_{\mathrm{r}}}{P_{\mathrm{n}}} \le x | P_{\mathrm{r}} > P_{\mathrm{th}}\right) \\ &= (1-p_1)(1-p_2)\frac{P(P_{\mathrm{th}} < P_{\mathrm{r}} \le P_{\mathrm{n}}x)}{1-P(P_{\mathrm{r}} \le P_{\mathrm{th}})} \\ &= (1-p_1)(1-p_2)\frac{F_{P_{\mathrm{r}}|d_{\mathrm{s}}}(P_{\mathrm{n}}x) - F_{P_{\mathrm{r}}|d_{\mathrm{s}}}(P_{\mathrm{th}})}{1-F_{P_{\mathrm{r}}|d_{\mathrm{s}}}(P_{\mathrm{th}})}, \end{aligned} \quad (15)$$

$$\begin{aligned} &f_{\mathrm{SINR_n}|(d_{\mathrm{s}},P_{\mathrm{r}}>P_{\mathrm{th}})}(x) \\ &= \frac{dF_{\mathrm{SINR_n}|(d_{\mathrm{s}},P_{\mathrm{r}}>P_{\mathrm{th}})}(x)}{\mathrm{d}x} \\ &= (1-p_1)(1-p_2)\frac{P_{\mathrm{n}} f_{P_{\mathrm{r}}|d_{\mathrm{s}}}(P_{\mathrm{n}}x)}{1-\int_0^{P_{\mathrm{th}}} f_{P_{\mathrm{r}}|d_{\mathrm{s}}}(y)\mathrm{d}y}. \end{aligned} \quad (16)$$

F. Derivation of QoS Metrics and Link Capacity

This subsection presents the definitions for PRP, PRR and link capacity.

1) Prp: the distribution of SINR when $D_{\mathrm{S}} = d_{\mathrm{s}}$ can be obtained from by (14) and (16):

$$\begin{aligned} f_{\mathrm{SINR}|(d_{\mathrm{s}},P_{\mathrm{r}}>P_{\mathrm{th}})}(x) &= f_{\mathrm{SINR_I}|(d_{\mathrm{s}},P_{\mathrm{r}}>P_{\mathrm{th}})}(x) \\ &\quad + f_{\mathrm{SINR_n}|(d_{\mathrm{s}},P_{\mathrm{r}}>P_{\mathrm{th}})}(x). \end{aligned} \quad (17)$$

From (17) the conditional CDF of SINR could be presented as

$$F_{\mathrm{SINR}|(d_{\mathrm{s}},P_{\mathrm{r}}>P_{\mathrm{th}})}(x) = \int_0^x f_{\mathrm{SINR}|(d_{\mathrm{s}},P_{\mathrm{r}}>P_{\mathrm{th}})}(t)\mathrm{d}t. \quad (18)$$

Transmissions in the same slot from vehicles within the interference range of the tagged vehicle, which cannot be detected by CSMA protocol, may also cause packet (message) collisions, this situation is called concurrent collision. The probability that there are no concurrent collisions with the transmission from R is derived as [22]

$$P_{\mathrm{con}|d_{\mathrm{s}}} = \exp(-\overline{n}_{\Sigma}), \quad (19)$$

where $\overline{n}_{\Sigma}$ is the average number of nodes transmitting in the concurrent slot in sensing range of receiving node.

The probability that the receiver with distance d_{s} to the tagged node accepts the message successfully if the measured SINR is bigger than the given threshold and the received signal should be stronger than the reception threshold P_{th}, which is expressed as

$$\begin{aligned} &\mathrm{PRP}(d_{\mathrm{s}},\theta) \\ &= P(\mathrm{SINR} \ge \theta | d_{\mathrm{s}}, P_{\mathrm{r}} > P_{\mathrm{th}}) P_{\mathrm{con}|d_{\mathrm{s}}} \\ &= P(\mathrm{SINR} \ge \theta | (d_{\mathrm{s}}, P_{\mathrm{r}} > P_{\mathrm{th}}) P(P_{\mathrm{r}} > P_{\mathrm{th}}) P_{\mathrm{con}|d_{\mathrm{s}}} \\ &= (1 - F_{\mathrm{SINR}|(d_{\mathrm{s}},P_{\mathrm{r}}>P_{\mathrm{th}})}(\theta)) \\ &\left(1 - \int_0^{P_{\mathrm{th}}} f_{P_{\mathrm{r}}|d_{\mathrm{s}}}(x)\mathrm{d}x\right) P_{\mathrm{con}|d_{\mathrm{s}}}. \end{aligned} \quad (20)$$

2) Prr: Define the Region of Interest (ROI) of a safety application as the size of the geographical region covered by those entities participating in the application, which is denoted as d_{ROI}. Different kinds of safety applications have different ROI sizes [41].

Packet Reception Ratio (PRR) (the percentage of receivers that are free from transmission errors) within ROI can be evaluated as

$$\mathrm{PRR}(d,\theta) = \frac{\int_0^d \beta(x)\mathrm{PRP}(x,\theta)\mathrm{d}x}{\int_0^d \beta(x)\mathrm{d}x}, d \le d_{\mathrm{ROI}}.$$

3) Link Capacity: the SINR distribution without D_{S} is used to obtain the link capacity distribution, and the PDF of D_{S} is deduced similar to deductions (2)–(8), The total D_{S}'s PDF can be expressed as

$$f_{D_{\mathrm{S}}}(x) = \frac{\beta(x)}{\int_0^{r_{\mathrm{E}}} \beta(z)\mathrm{d}z}. \quad (21)$$

The SINR's PDF and CDF can be derived as

$$\begin{aligned} f_{\mathrm{SINR}|(P_{\mathrm{r}}>P_{\mathrm{th}})}(x) &= \int_0^{r_{\mathrm{E}}} f_{\mathrm{SINR}|(d_{\mathrm{s}},P_{\mathrm{r}}>P_{\mathrm{th}})}(x) f_{D_{\mathrm{S}}}(t)\mathrm{d}t, \\ F_{\mathrm{SINR}|(P_{\mathrm{r}}>P_{\mathrm{th}})}(x) &= \int_0^x f_{\mathrm{SINR}|(P_{\mathrm{r}}>P_{\mathrm{th}})}(t)\mathrm{d}t. \end{aligned} \quad (22)$$

The link capacity of the channel represents the upper limit of the channel transmission rate (bits per second), which is given by Shannon formula:

$$\begin{aligned} C &= W \log_2(1+\mathrm{SINR}), \\ &\quad C: \text{link capacity}, \\ &\quad W: \text{network bandwidth}. \end{aligned} \tag{23}$$

CDF of link capacity can be obtained by using SINR's CDF and Shannon formula:

$$\begin{aligned} F_C(x) &= P(W\log_2(1+\mathrm{SINR}) < x) \\ &= F_{\mathrm{SINR}|(P_\mathrm{r}>P_\mathrm{th})}(2^{x/W}-1). \end{aligned} \tag{24}$$

Further, we can get the PDF and expectation of link capacity as follows:qn26

$$\begin{aligned} f_C(x) &= \frac{\ln 2}{W}\cdot(2^{x/W}) f_{\mathrm{SINR}|(P_\mathrm{r}>P_\mathrm{th})}(2^{x/W}-1), \\ E(C) &= \int_0^\infty x f_C(x)\mathrm{d}x. \end{aligned} \tag{25}$$

III. QoS and Capacity of Beacon Message Broadcast in Two-Dimensional VANET

This section presents the analytic model for 2-D intersection, and the CDF of SINR is derived similar to the II-B. Without loss of generality, two cases accounting for locations geometry between tagged transmitter and receiver are utilized to show how to derive PRP, PRR, and capacity analytically. At each case, the combinations between the number of interference areas and whether there exist interference node transmitting are gathered at $2^4 = 16$, where the number of interference areas equals 4. The analyses of 2-D are more complex compared with 1-D since various combinations need to be traced.

A. Assumptions

In addition to the same assumptions as to the 1-D case, the following assumptions apply to the 2-D intersection scenario: (1) Each crossing road has one lane per direction so that each intersection can be approximated by cross lines. The intersection is widely separated from the other intersection, so there is no overlap of the communication range. (2) Distance between intersections far exceeds the node's transmission range. (3) The impact of interferes on the tagged receiver node R can be approximated by the shaded region of four sides shown in Fig. 2 or Fig. 3.

Assuming that the coordinate of the intersection is (0,0). Given a transmitting node T placed in $(x_0, 0)$ (see Fig. 2), R is one of the receivers within ROI of node T for the safety application. The position of R is either $(x_\mathrm{r}, 0)$ or $(0, y_\mathrm{r})$ $(|x_\mathrm{r} - x_0| \leq d_\mathrm{ROI}, y_\mathrm{r}^2 + x_0^2 \leq d_\mathrm{ROI}^2)$, we need to study CDF of SINR for each case. The implication of SINR, $\mathrm{SINR_I}$, and $\mathrm{SINR_n}$ is the same as that of 1-D case.

B. Case 1 R in $(x_\mathrm{R}, 0)$

As shown in Fig. 2, assuming that the interference $I_1(I_2)$ is within the right(left) shaded region on the X-axis with distance to T as $[r_\mathrm{E}, 2r_\mathrm{E}]$, and there are $l(l')$ nodes in this region; the interference $I_3(I_4)$ is within the up(down) shaded region on the Y-axis with distance to T as $[r_\mathrm{E}, 2r_\mathrm{E}]$, and there are $l''(l''')$ nodes

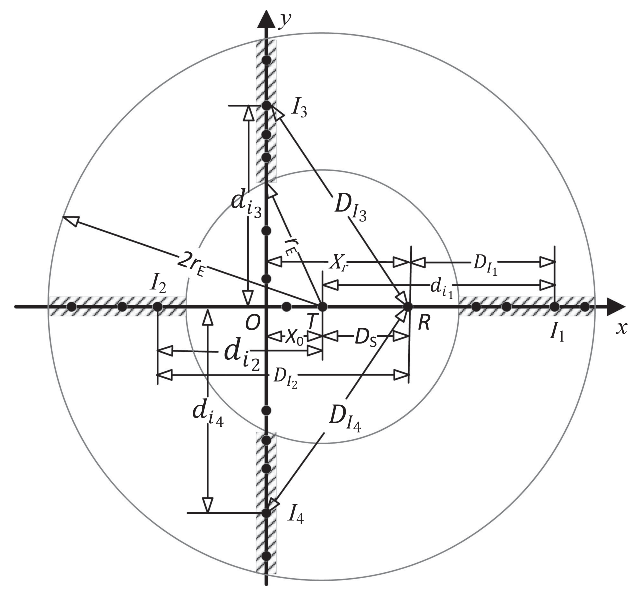

Fig. 2. A general interfering scenario for intersection as receiving node is in $(x_\mathrm{r}, 0)$.

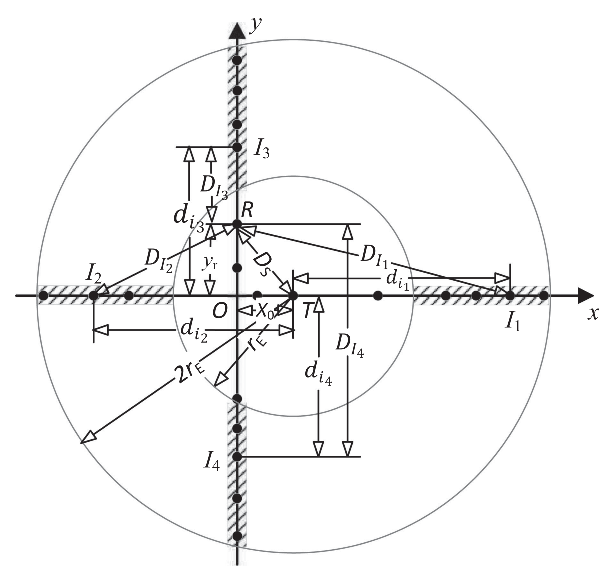

Fig. 3. A general interfering scenario for intersection as receiving node is in $(0, y_\mathrm{r})$.

in this region. $D_{I_k}(k = 1, 2, 3, 4)$ denote the distance between the node of I_k and the R, D_S denotes the distance between the T and R.

1) The Interference Distance Distribution: The distribution of I_1 and I_2 is the same as in 1-D case, but the coordinate of the origin is changed from T to O, and $X_0 = x_0(x_0 + d_s = x_r)$. Transform coordination x_0 in (8) and (9) to obtain the PDF of I_1 and I_2:

$$f_{D_{I_1}|(x_0,x_r)}(x) = \frac{\beta(x + x_\mathrm{r})}{\int_{x_0+r_\mathrm{E}}^{x_0+2r_\mathrm{E}} \beta(z)\mathrm{d}z}. \tag{26}$$

$$f_{D_{I_2}|(x_0,x_r)}(x) = \frac{\beta(x_\mathrm{r} - x)}{\int_{x_0-2r_\mathrm{E}}^{x_0-r_\mathrm{E}} \beta(z)\mathrm{d}z}. \tag{27}$$

The PDF of I_3, $f_{D_{I_3}|(x_0,x_\mathrm{r})}(y)$ formulated as (28) and the concrete deductions are presented in Appendix A.

$$f_{D_{I_3}|(x_0,x_r)}(y) = \frac{\beta(\sqrt{y^2-x_r^2})}{\int_{\sqrt{r_\mathrm{E}^2-x_0^2}}^{\sqrt{4r_\mathrm{E}^2-x_0^2}} \beta(z)\mathrm{d}z}. \tag{28}$$

Considering that upside and downside of the vertical axis are symmetrical to each other, the PDF of D_{I_4} is equal to PDF of D_{I_3}.

2) PDF of SINR With Interference: The CDF of interference power P_{I_1}, P_{I_2}, and P_{I_3} received at R could be presented as

$$\begin{aligned}
&F_{P_{I_1}|(x_0,x_\mathrm{r})}(x) = P(P_{I_1} \le x|(x_0,x_\mathrm{r}))\\
&\quad = \int_{t'=0}^{x}\int_{r_\mathrm{E}-d_\mathrm{s}}^{2r_\mathrm{E}-d_\mathrm{s}} f_{P_\mathrm{r}|D_{I_1}}(t')f_{D_{I_1}|(x_0,x_\mathrm{r})}(t)\mathrm{d}t\mathrm{d}t',\\
&F_{P_{I_2}|(x_0,x_\mathrm{r})}(x) = P(P_{I_2} \le x|(x_0,x_\mathrm{r}))\\
&\quad = \int_{t'=0}^{x}\int_{r_\mathrm{E}+d_\mathrm{s}}^{2r_\mathrm{E}+d_\mathrm{s}} f_{P_\mathrm{r}|D_{I_2}}(t')f_{D_{I_2}|(x_0,x_\mathrm{r})}(t)\mathrm{d}t\mathrm{d}t',\\
&F_{P_{I_3}|(x_0,x_\mathrm{r})}(y) = P(P_{I_3} \le y|(x_0,x_\mathrm{r}))\\
&\quad = \int_{t'=0}^{y}\int_{\sqrt{r_\mathrm{E}^2-x_0^2+x_r^2}}^{\sqrt{4r_\mathrm{E}^2-{x_0}^2+x_r^2}} f_{P_\mathrm{r}|D_{I_3}}(t')f_{D_{I_3}|(x_0,x_\mathrm{r})}(t)\mathrm{d}t\mathrm{d}t'.
\end{aligned}$$

Then the PDF of $P_{I_1} \sim P_{I_4}$ can be derived as

$$\begin{aligned}
f_{P_{I_1}|(x_0,x_\mathrm{r})}(x) &= \frac{\mathrm{d}F_{P_{I_1}|(x_0,x_\mathrm{r})}(x)}{\mathrm{d}x},\\
f_{P_{I_2}|(x_0,x_\mathrm{r})}(x) &= \frac{\mathrm{d}F_{P_{I_2}|(x_0,x_\mathrm{r})}(x)}{\mathrm{d}x},\\
f_{P_{I_3}|(x_0,x_\mathrm{r})}(y) &= \frac{\mathrm{d}F_{P_{I_3}|(x_0,x_\mathrm{r})}(y)}{\mathrm{d}y}.
\end{aligned}$$

From the symmetry, we get the following results:

$$f_{P_{I_4}|(x_0,x_\mathrm{r})}(y) = f_{P_{I_3}|(x_0,x_\mathrm{r})}(y).$$

The combinations between the number of interferer areas and whether there exist interferers in each area are total $2^4 = 16$, and 15 types of combinations with interference of total 16 combinations could be derived. When there are multiple interferences, the PDF of interference power at the receiving node R is the convolution sum of PDFs of other interference powers. The following is an example of the expression of convolution sum in some cases, other cases are similar and can be omitted.

$$\begin{aligned}
f_{P_{I_1I_3}|(x_0,x_\mathrm{r})}(x) &= \int_0^\infty f_{P_{I_1}|(x_0,x_\mathrm{r})}(x-t)f_{P_{I_3}|(x_0,x_\mathrm{r})}(t)\mathrm{d}t,\\
f_{P_{I_2I_4}|(x_0,x_\mathrm{r})}(x) &= \int_0^\infty f_{P_{I_2}|(x_0,x_\mathrm{r})}(x-t)f_{P_{I_4}|(x_0,x_\mathrm{r})}(t)\mathrm{d}t,\\
f_{P_{I_{1-4}}|(x_0,x_\mathrm{r})}(x) &= \int_0^\infty f_{P_{I_1I_3}|(x_0,x_\mathrm{r})}(x-t)f_{P_{I_2I_4}|(x_0,x_\mathrm{r})}(t)\mathrm{d}t,\\
f_{P_{I_1I_2I_4}|(x_0,x_\mathrm{r})}(x) &= \int_0^\infty f_{P_{I_1}|(x_0,x_\mathrm{r})}(x-t)f_{P_{I_2I_4}|(x_0,x_\mathrm{r})}(t)\mathrm{d}t.
\end{aligned} \tag{29}$$

Let p_1, p_2, p_3 and p_4 indicate the probability of interferences in the right, up, left and down shaded regions, respectively. Using the same method as (11), (12), the following formulas can be obtained:

$$\begin{aligned}
p_1 &= 1 - \exp\left(-p_\mathrm{t}\int_{x_0+r_\mathrm{E}}^{x_0+2r_\mathrm{E}} \beta(x)\mathrm{d}x\right),\\
p_3 &= 1 - \exp\left(-p_\mathrm{t}\int_{x_0-r_\mathrm{E}}^{x_0-2r_\mathrm{E}} \beta(x)\mathrm{d}x\right),\\
p_2 = p_4 &= 1 - \exp\left(-p_\mathrm{t}\int_{\sqrt{r_\mathrm{E}^2-x_0^2}}^{\sqrt{4r_\mathrm{E}^2-x_0^2}} \beta(y)\mathrm{d}y\right).
\end{aligned} \tag{30}$$

The p_t is given by (10). According to the PDF of interference power in 15 cases with interference and the probability of each case, the average PDF of interference power with interference is obtained by using the full probability formula.

$$\begin{aligned}
f_{P_I|(x_0,x_\mathrm{r})}(x) &= \prod_{i=1}^{4} p_i f_{P_{I_{1-4}}|(x_0,x_\mathrm{r})}(x)\\
&+ \sum_{i=1}^{4}\left[(1-p_i)\cdot\prod_{\substack{j=1\\j\neq i}}^{4} p_j \cdot f_{P_{\prod_{j=1,\, j\neq i}^{4} I_j}|(x_0,x_\mathrm{r})}(x)\right]\\
&+ \sum_{i=1}^{4}\left[p_i\prod_{\substack{j=1\\j\neq i}}^{4}(1-p_j)\cdot f_{P_{I_i}|(x_0,x_\mathrm{r})}(x)\right]\\
&+ \sum_{i=1}^{3}\left[\sum_{j=i+1}^{4} p_ip_j\prod_{\substack{k=1\\k\neq i\\k\neq j}}^{4}(1-p_k)f_{P_{I_iI_j}|(x_0,x_\mathrm{r})}(x)\right].
\end{aligned} \tag{31}$$

The conditional PDF of SINR with interference is

$$\begin{aligned}
&f_{\mathrm{SINR_I}|(x_0,x_\mathrm{r},P_\mathrm{r}>P_\mathrm{th})}(x)\\
&\quad = \int_{\mathrm{Max}\{\frac{P_\mathrm{th}}{x},P_\mathrm{th}\}}^{\infty} t\cdot f_{P_\mathrm{r}|(x_0,x_\mathrm{r})}(t\cdot x)f_{P_\mathrm{I}|(x_0,x_\mathrm{r})}(t)\mathrm{d}t,
\end{aligned} \tag{32}$$

3) PDF of SINR Without Interference: Similar to (15), (16), the PDF of SINR without interference can be obtained as

$$\begin{aligned}
&f_{\mathrm{SINR_n}|(x_0,x_\mathrm{r},P_\mathrm{r}>P_\mathrm{th})}(x)\\
&\quad = \prod_{i=1}^{4}(1-p_i)\frac{P_{I_\mathrm{n}}f_{P_\mathrm{r}|(x_0,x_\mathrm{r})}(P_{I_\mathrm{n}}x)}{1-\int_0^{P_\mathrm{th}} f_{P_\mathrm{r}|(x_0,x_\mathrm{r})}(y)\mathrm{d}y}.
\end{aligned} \tag{33}$$

4) QoS Metrics: The conditional PDF of SINR can be presented as

$$\begin{aligned}
f_{\mathrm{SINR}|(x_0,x_\mathrm{r},P_\mathrm{r}>P_\mathrm{th})}(x) &= f_{\mathrm{SINR_I}|(x_0,x_\mathrm{r},P_\mathrm{r}>P_\mathrm{th})}(x)\\
&\quad + f_{\mathrm{SINR_n}|(x_0,x_\mathrm{r},P_\mathrm{r}>P_\mathrm{th})}(x).
\end{aligned} \tag{34}$$

The SINR's conditional CDF could be presented as

$$F_{\mathrm{SINR}|(x_0,x_\mathrm{r},P_\mathrm{r}>P_\mathrm{th})}(x) = \int_0^x f_{\mathrm{SINR}|(x_0,x_\mathrm{r},P_\mathrm{r}>P_\mathrm{th})}(t)\mathrm{d}t. \tag{35}$$

Use the same method as (21), the PDF of $D_{\rm S}$ can be obtained by

$$f_{D_{\rm S}}(x)=\frac{\beta(x)}{\int_{x_0}^{r_{\rm E}+x_0}\beta(z){\rm d}z}.$$

The SINR's PDF and CDF can be derived as

$$\begin{aligned}f_{{\rm SINR}|(P_{\rm r}>P_{\rm th})}(x)&=\int_0^{r_{\rm E}}f_{{\rm SINR}|(x_0,x_{\rm r},P_{\rm r}>P_{\rm th})}(x)f_{D_{\rm S}}(t){\rm d}t,\\ F_{{\rm SINR}|(P_{\rm r}>P_{\rm th})}(x)&=\int_0^{x}f_{{\rm SINR}|(P_{\rm r}>P_{\rm th})}(t){\rm d}t.\end{aligned}\tag{36}$$

Then the PRP with distance $d_{\rm s}$ to the tagged node and the PRR within ROI can be evaluated as

$$\begin{aligned}{\rm PRP}(d_{\rm s},\theta)=&\left(1-F_{{\rm SINR}|\{x_0,x_{\rm r},P_{\rm r}>P_{\rm th}\}}(\theta)\right)\\&\times\left(1-\int_0^{P_{\rm th}}f_{P_{\rm r}|d_{\rm s}}(x){\rm d}x\right)\times P_{{\rm con}|(x_0,x_r)},\\ P_{{\rm con}|d_{\rm s}}=&\exp\left(-\overline{n}_{\Sigma_{(x_0,x_r)}}\right),\\ {\rm PRR}(d,\theta)=&\frac{\int_{x_0-d}^{x_0+d}\beta(x){\rm PRP}(x,\theta){\rm d}x}{\int_{x_0-d}^{x_0+d}\beta(x){\rm d}x},d\le d_{\rm ROI}.\end{aligned}\tag{37}$$

C. Case 2 R in $(0,y_{\rm r})$

As shown in Fig. 3, assuming that the interference $I_1(I_2)$ is within the right(left) shaded region on the X-axis with distance to T as $[r_{\rm E},2r_{\rm E}]$, and there are $l(l')$ nodes in this region; the interference $I_3(I_4)$ is within the up(down) shaded region on the Y-axis with distance to T as $[r_{\rm E},2r_{\rm E}]$, and there are $l''(l''')$ nodes in this region. $D_{I_k}(k=1,2,3,4)$ denote the distance between the node of I_k and the R, $D_{\rm S}$ denotes the distance between the T and R.

1) The Interference Distance Distribution: $f_{D_{I_1}|(x_0,y_{\rm r})}(x)$ and $f_{D_{I_3}|(x_0,y_{\rm r})}(y)$ denote the PDF of D_{I_1} and D_{I_3}, respectively, which are formulated as in (38). And, the derivations of (38) are presented as Appendix B.

$$\begin{aligned}f_{D_{I_1}|(x_0,y_{\rm r})}(x)&=\frac{\beta(\sqrt{x^2-y_{\rm r}^2})}{\int_{r_{\rm E}+x_0}^{2r_{\rm E}+x_0}\beta(z){\rm d}z},\\ f_{D_{I_3}|(x_0,y_{\rm r})}(y)&=\frac{\beta(y+y_{\rm r})}{\int_{\sqrt{r_{\rm E}^2-x_0^2}}^{\sqrt{4r_{\rm E}^2-x_0^2}}\beta(z){\rm d}z}.\end{aligned}\tag{38}$$

The derivations of $f_{D_{I_2}|(x_0,y_{\rm r})}(x)$ as well as $f_{D_{I_4}|(x_0,y_{\rm r})}(y)$ are similar with $f_{D_{I_1}|(x_0,y_{\rm r})}(x)$ and $f_{D_{I_3}|(x_0,y_{\rm r})}(y)$, which is formulated as (39).

$$\begin{aligned}f_{D_{I_2}|(x_0,y_{\rm r})}(x)&=\frac{\beta(-\sqrt{x^2-y_{\rm r}^2})}{\int_{x_0-2r_{\rm E}}^{x_0-r_{\rm E}}\beta(z){\rm d}z},\\ f_{D_{I_4}|(x_0,y_{\rm r})}(y)&=\frac{\beta(y_{\rm r}-y)}{\int_{-\sqrt{4r_{\rm E}^2-x_0^2}}^{-\sqrt{r_{\rm E}^2-x_0^2}}\beta(z){\rm d}z}.\end{aligned}\tag{39}$$

2) CDF of SINR and QoS Metrics: The CDF and PDF of I_k's interference power P_{I_k} received at R could be presented as

$$\begin{aligned}F_{P_{I_1}|(x_0,y_{\rm r})}(x)&=P(P_{I_1}\le x|(x_0,y_{\rm r}))\\&=\int_{t'=0}^{x}\int_{\sqrt{(r_{\rm E}+x_0)^2+y_r^2}}^{\sqrt{(2r_{\rm E}+x_0)^2+y_r^2}}f_{P_{\rm r}|D_{I_1}}(t')f_{D_{I_1}|(x_0,y_{\rm r})}(t){\rm d}t{\rm d}t',\\ F_{P_{I_2}|(x_0,y_{\rm r})}(x)&=P(P_{I_2}\le x|(x_0,y_{\rm r}))\\&=\int_{t'=0}^{x}\int_{\sqrt{r_{\rm E}^2-x_0^2}+y_{\rm r}}^{\sqrt{4r_{\rm E}^2-x_0{}^2}+y_{\rm r}}f_{P_{\rm r}|D_{I_2}}(t')f_{D_{I_2}|(x_0,y_{\rm r})}(t){\rm d}t{\rm d}t',\\ F_{P_{I_3}|(x_0,y_{\rm r})}(y)&=P(P_{I_3}\le y|(x_0,y_{\rm r}))\\&=\int_{t'=0}^{y}\int_{\sqrt{r_{\rm E}^2-x_0^2}-y_{\rm r}}^{\sqrt{4r_{\rm E}^2-x_0{}^2}-y_{\rm r}}f_{P_{\rm r}|D_{I_3}}(t')f_{D_{I_3}|(x_0,y_{\rm r})}(t){\rm d}t{\rm d}t',\\ F_{P_{I_4}|(x_0,y_{\rm r})}(y)&=P(P_{I_4}\le y|(x_0,y_{\rm r}))\\&=\int_{t'=0}^{y}\int_{\sqrt{r_{\rm E}^2-x_0^2}+y_{\rm r}}^{\sqrt{4r_{\rm E}^2-x_0{}^2}+y_{\rm r}}f_{P_{\rm r}|D_{I_4}}(t')f_{D_{I_4}|(x_0,y_{\rm r})}(t){\rm d}t{\rm d}t'.\end{aligned}$$

Then the PDF and CDF of SINR can be obtained by using a method similar to (29)–(36):

$$\begin{aligned}f_{{\rm SINR}|(P_{\rm r}>P_{\rm th})}(x)&=\int_0^{r_{\rm E}}f_{{\rm SINR}|(x_0,y_{\rm r},P_{\rm r}>P_{\rm th})}(x)f_{D_{\rm S}}(t){\rm d}t,\\ F_{{\rm SINR}|(P_{\rm r}>P_{\rm th})}(x)&=\int_0^{x}f_{{\rm SINR}|(P_{\rm r}>P_{\rm th})}(t){\rm d}t,\end{aligned}$$

and

$$f_{D_{\rm S}}(y)=\frac{y}{\sqrt{y^2-x_0^2}}\int_0^{\sqrt{y^2-x_0^2}}\frac{\beta(t)}{\int_0^{r_{\rm E}}\beta(z){\rm d}z}{\rm d}t.$$

The PRP with distance $d_{\rm s}$ to the tagged node and the PRR within ROI can be evaluated as

$$\begin{aligned}{\rm PRP}(x_0,y_{\rm r},\theta)&=P\left({\rm SINR}\ge\theta|(x_0,y_{\rm r})\right)P(P_{\rm r}>P_{\rm th})\\&=\left(1-F_{{\rm SINR}|(x_0,y_r,P_{\rm r}>P_{\rm th})}(\theta)\right)\\&\quad\times\left(1-\int_0^{P_{\rm th}}f_{P_{\rm r}|d_{\rm s}}(x){\rm d}x\right)\times P_{{\rm con}|(x_0,y_r)},\\ P_{{\rm con}|d_{\rm s}}&=\exp\left(-\overline{n}_{\Sigma_{(x_0,y_{\rm r})}}\right),\\ {\rm PRR}(d,\theta)&=\frac{\int_{-\sqrt{d^2-x_0^2}}^{\sqrt{d^2-x_0^2}}\beta(y){\rm PRP}(x_0,y,\theta){\rm d}y}{\int_{\sqrt{d^2-x_0^2}}^{\sqrt{d^2-x_0^2}}\beta(x){\rm d}x},\\ x_0&\le d\le\sqrt{d_{\rm ROI}^2-x_0^2}.\end{aligned}\tag{40}$$

D. Capacity Derivation

The solutions of PDF and expectation of link capacity are the same as those of 1-D, and (23)–(25) are also applicable to 2-D intersection.

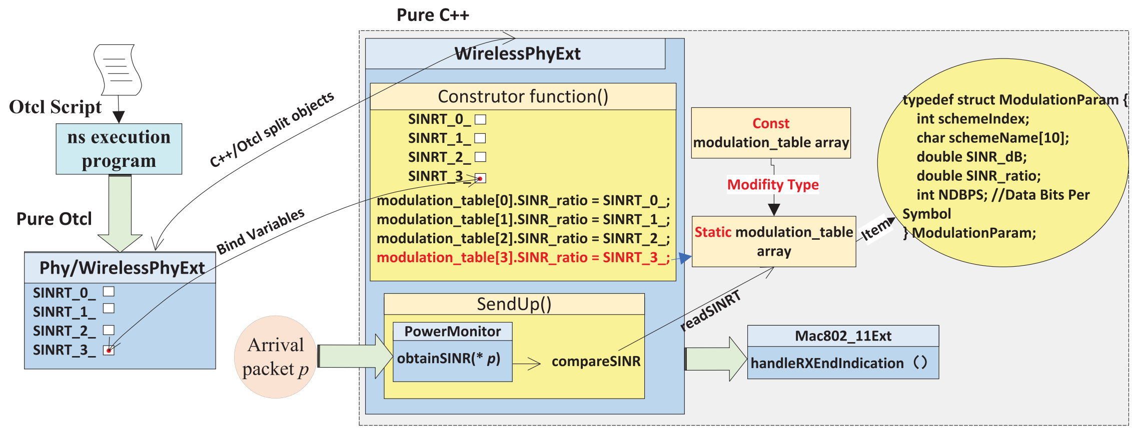

Fig. 4. Architecture of the NS2 simulation.

TABLE I
MODULATION SCHEMES, R_{d}S, AND SINRTS OF IEEE 802.11P IN NS2

#	Modulation scheme	R_{d} (Mbps)	SINRT	SINRT (dB)
0	BPSK	3	3.1623	5
1	QPSK	6	6.3096	8
2	QAM16	12	31.6228	15
3	QAM64	24	316.2278	25

IV. NS2 SIMULATION AND SETTINGS

We adopt NS2 simulator version 2.35 to validate the theoretical model. Some modifications to the source code of NS2 for adjusting SINRTs are made to allow the user to define SINRTs. Furthermore, we compare the performance of the static simulation scenario and the mobility simulation scenario, where the mobility traffic is generated by SUMO and NS2 mobility tool, respectively. Results show that there are almost no differences between the performance metrics obtained by statistics in the mobility scene and the static simulation scene. Therefore, we adopt static scene simulation in subsequent NS2 simulation experiments for verifying the theoretical model.

A. Flexible SINR Threshold Settings

The NS2 adopts the SINR based method to determine whether an incoming signal is received or not by comparing the SINR of the signal and the customized SINRT stored in $modulation\_table$ variable. SINRTs are fixed values in terms of the modulation schemes and corresponding data rate (R_{d}) as shown in Table I. Therefore, we redesign the $WirelessphyExt$ class by modifying the $modulation\_table$ variable type and its constructor function in NS2 to enable the flexible SINRTs setting by user-programmable Tcl script. The specific details are shown in Fig. 4.

B. Simulation Parameter Settings

In our experiment, we consider the specific DSRC VANETs in both 1-D highway with a length of 5 km and the 2-D intersection road with a length of 1250 m on each of the crossing roads for safety message dissemination, respectively. Each vehicle in the network is equipped with DSRC capability. The communication

TABLE II
SIMULATION PARAMETERS

Parameters	Values
Carrier frequency	5.9 GHz
Channel bandwidth	10 MHz
Transmit power	0.155 Watts
Average sensing range r_{E}	300 m
Carrier sensing threshold P_{th}	2.81838e-11 Watts
Reference distance d_0	100 m
Noise floor	-99 dBm
Transmit gain G_{t}	1.0
Receive gain R_{r}	1.0
η	7.29e-10
PLCP header T_{H3}	4 µs
CW W-1	15
Path loss exponent α	2
DIFS	64 µs
Packet length PL	200 bytes
Slot time σ	16 µs
Data rate R_{d}	24 Mbps
PHY preamble T_{H1}	40 µs
MAC header T_{H2}	272 bits
Packet generation interval T_{c}	0.1 s
Fading parameter m	$\begin{cases} 3, & \text{for } \Delta \le 50 \text{ m} \\ 1.5, & \text{for } 50 \text{ m} < \Delta \le 100 \text{ m} \\ 1, & \text{for } \Delta > 100 \text{ m} \end{cases}$

vehicles are Poisson distributed with piecewise constant densities, which are the functions of distances Δ ($\Delta = x$ or $\Delta = y$) to a tagged vehicle as follows.

$$\beta(\Delta) = \begin{cases} 1.5\beta_{\mathrm{av}}, & -50 \text{ m} \le \Delta \le 50 \text{ m} \\ \beta_{\mathrm{av}}, & \Delta < -100 \text{ m or } \Delta > 100 \text{ m} \\ 0.5\beta_{\mathrm{av}}, & \text{others,} \end{cases}$$

where β_{av} is set to 0.066 vehicles/meter, 0.132 vehicles/meter, 0.2 vehicles/meter, and 0.5 vehicles/meter, respectively.

We list the critical simulation parameters for the 1-D highway and the 2-D intersection road as shown in Table II. The simulation parameter settings are consistent with the theoretical calculations. According to [35], transmission range, carrier sensing range, and interference range for research are set 300 m, respectively. Carrie sensing threshold P_{th} is calculated by *Nakagami* model, which equals 2.81838e-11 Watts, and the

TABLE III
VEHICLE PARAMETER SETTINGS IN SUMO

Parameters	Values	Parameters	Values
Acceleration	2.9 m/s^2	Deceleration	7.5 m/s^2
Emergency braking speed	10 m/s^2	Mean speed	25 m/s (90 km/h)
Maximum speed	33 m/s (120 km/h)	Minimum speed	18 m/s (60 km/h)
Vehicle length	4.3 m	Sample step	1 ms

receiving power threshold and the power monitor threshold in NS2 are also set 2.81838e-11 Watts, respectively.

C. Mobility Scenario Simulations for VANETs

Traffic simulation software SUMO can mimic the realistic scene in which the vehicles move at a given speed. NS2 also provides a simple build-in mobility model to drive the movement of nodes. We implement two mobility traffic scenarios by SUMO and NS2's build-in mobility model.

In SUMO, we generate a two-lane, two-way highway scenario with the length of 5 km, enabling relative speed between vehicles, and the width of each lane is 3.2 m. All vehicles parameter settings are shown in Table III. Each vehicle updates the speed every 10 ms, and the speed of all vehicles follows the uniform distribution for the mean speed 90 km/h (i.e., 25 m/s) with the variance of $2\,(\mathrm{m/s})^2$. The driving speed changes as it approaches the safety distance with the vehicle ahead, thereby the inter-vehicle distance changes and can be regarded as approximately following NHPP. SUMO records the positions of vehicles at the sample step of 1 ms. The log files formed by the vehicle positions at different times are input into NS2 programs to simulation the mobility network scenario.

The mobility scenario of NS2 build-in mobility model is set as a one-way highway driving right with the length of 6 km, and the vehicles following the NHPP distribution with piecewise constant densities are put within the left 5 km of the road, and the simulation ends within 5 s. The other parameters are utilized similarly to SUMO.

D. Comparison Results Between Static Scene Simulation and Mobility Scene Simulation

Fig. 5 shows the PRP comparison results of the static scene simulation and two mobility scene simulations at the density of 0.132 vehicles/meter. The results show that the static scene simulation can obtain almost the same results as mobility scene simulations at the given receiving distance d_s and the SINRT. [10] also pointed out that the vehicles can be considered static during the period of transmitting a packet. Obviously, the static scenario simulation costs less time compared with the mobility scenarios simulation, so we adopt a static scenario simulation in the next comparisons.

V. THEORETICAL RESULTS ANALYSIS AND VALIDATION

In this section, we firstly compare the time complexity of the theoretical model between the order statistic and unordered.

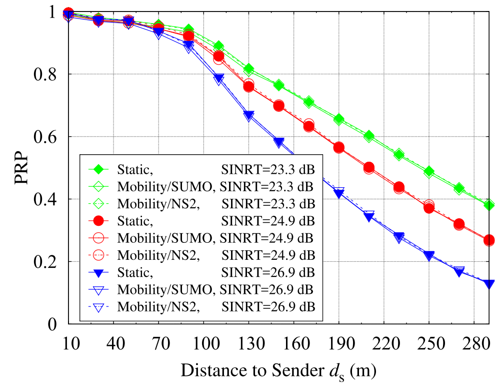

Fig. 5. PRP of static and mobility 1-D scenarios at the density of 0.132 vehicles/meter and the communication range of 300 m.

Secondly, we make the reliability cross-validations between the analytic model and NS2 simulation for the scenarios at 1-D as well as 2-D intersection to guarantee the accuracy of the analytic model. QoS metrics, including PRP, PRR, and SINR distribution at various VANET scenarios are obtained. Thirdly, we further compare the PRP of two scenes at 2-D and 1-D. Finally, the link capacity distribution in 1-D and 2-D VANETs are obtained by numerical computation.

The simulation scenarios include 1-D and two 2-D intersection scenes. Specifically, two types of 2-D intersection scenarios are considered since the closer the receiver is to the intersection, the more interference should be generated. In the first scenario, the sender is assumed at the intersection, and the vehicle node at the distance d_s from the intersection on the X-axis is the receiver. In the second scenario, the receiver is assumed at the intersection, and the vehicle node at the distance d_s from the intersection on the negative X-axis is the sender. All scenarios regard different densities covering the 0.066 vehicles/meter as low density, 0.132 vehicles/meter, 0.2 vehicles/meter as medium density, and 0.5 vehicles/meter as high density, respectively. At each density, we choose five values as SINRTs to observe the QoS metrics: 23.3 dB (215), 24.9 dB (315), 26.9 dB (500), 28.5 dB (700), and 30.0 dB (1000), respectively. In NS2 simulation, the experiment with the same density and the SINRT was performed ten times. The average value of ten PRP/PRR is used as the simulation results of PRPs/PRRs. The parameter settings are given in Section IV.

The results of various experiments pave the way to explore the accuracy of the proposed model for 1-D as well as 2-D VANETs, to analyze the effect of receiving distance d_s and SINRT on the reliability.

A. Time Complexity of Numerical Analysis

The computation efficiency of the SINR distribution based on order statistics and unordered at 1-D highway is given by the experiments. We adopt Monte Carlo integration and MPI parallel framework to implement the numerical programs calculation PRP to improve the computing speed. The programs are running on the MPI cluster composed of homogeneous nodes organized

TABLE IV
COMPARISONS OF COMPUTING TIME AND ACCURACY UNDER DIFFERENT INTERPOLATION NUMBERS

Cases		**1000**	**3000**	**5000**
Time (hour)	Ordered	9.98e-04	2.25e-03	3.51e-03
	Unordered	20.8	41.82	61.36
Integral error	Ordered	1.19e-04	4.56e-05	2.64e-05
	Unordered	1.38e-04	3.41e-05	2.13e-05

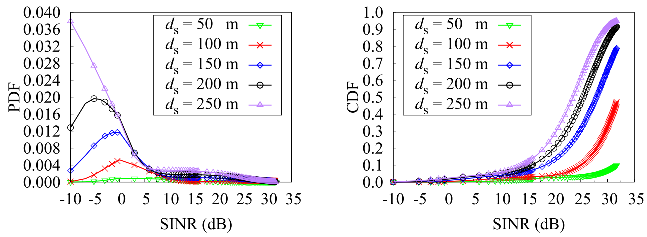

(a) (b)

Fig. 6. PDF and CDF of SINR in 1-D with the density of 0.132. (a) PDF of SINR. (b) CDF of SINR.

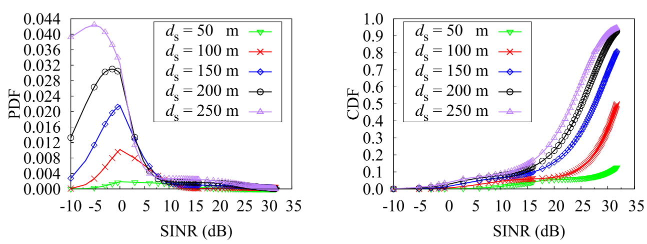

(a) (b)

Fig. 7. PDF and CDF of SINR in 2-D with the receiver at the intersection for the density of 0.132. (a) PDF of SINR. (b) CDF of SINR.

by Intel MPI 5.1.2. The hardwares of each node in the MPI cluster include Intel E5-2660 2.60 GHz CPU and 32 GB memory with 20 cores CPU for numerical integration.

Monte Carlo integration needs large enough sampling points to ensure accuracy. The number of sampling is 1000, 3000, and 5000 times, respectively. SINRT value θ is set as 4, and signal propagation distance d_{s} is set as 50 m. The execution time of single interpolation for ordered and unordered by Monte Carlo integration are 38.1328 ms, 736 462 ms, respectively. Table IV presents the comparisons of computing time and accuracy when the number of sampling points is 1000, 3000, and 5000 times, respectively. It is clear to see from Table IV that the ordered model has dramatically reduced the computational complexity compared with the unordered.

B. Cross-Validation Between Theoretical Calculation and NS2 Simulation

1) Pdf, Cdf of Sinr: We compute the PDF and CDF of SINR within 1500 (31.8 dB) at a 1-D scene and two 2-D scenes. Fig. 6 and Fig. 7 present the PDF and CDF of SINR in 1-D and 2-D scene with the receiver at an intersection for the density of

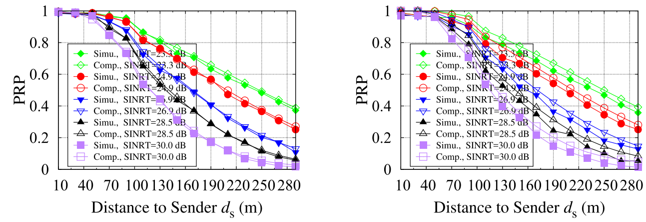

(a) (b)

Fig. 8. PRP comparisons between the theoretical model and the simulation in the 1-D scene. (a) The density is 0.066. (b) The density is 0.132.

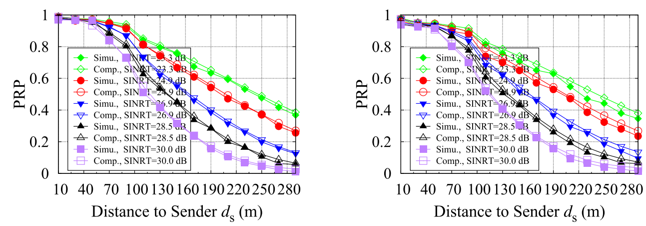

(a) (b)

Fig. 9. PRP comparisons between the theoretical model and the simulation where the sender is at a 2-D intersection. (a) The density is 0.066. (b) The density is 0.132.

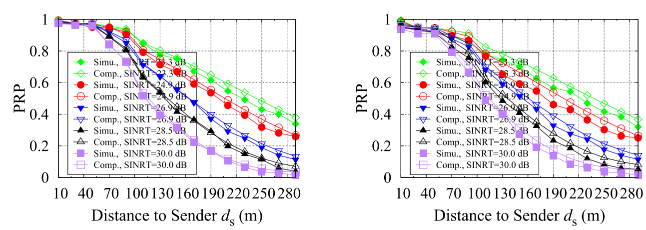

(a) (b)

Fig. 10. PRP comparisons between the theoretical model and the simulation where the receiver is at a 2-D intersection. (a) The density is 0.066. (b) The density is 0.132.

0.132 vehicles/meter. The results show that the smaller d_{s}, the larger average value of SINR, and otherwise, the larger d_{s}, the smaller the mean of SINR. The small d_{s} value means the small attenuation power for receiver and thus SINR becomes large, which is consistent with the results from Fig. 6 and Fig. 7.

2) PRP, PRR of 1-D, 2-D With Low, Medium Density: Fig. 8 – Fig. 10 show the PRP comparisons between the analytical model and NS2 simulation at the density equaling 0.066 vehicles/meter and 0.132 vehicles/meter in 1-D, 2-D with the sender at an intersection, and 2-D with the receiver at an intersection. It can be seen that the analytical results are consistent with the simulations results with various d_{s} as well as SINRT values at each density, and it also shows the d_{s} and the SINRTs affect the PRP. d_{s} starts from 10 m until 300 m at the 20 m interval, it is obvious from the figures that PRPs decrease with the increasing d_{s}. The increasing d_{s} suffers more channel attenuation, resulting in lower received power, which will further reduce the SINR values for the receiver, as a result it could not satisfy the requirement of SINRTs. Thus, the increasing d_{s} definitely cause the PRP

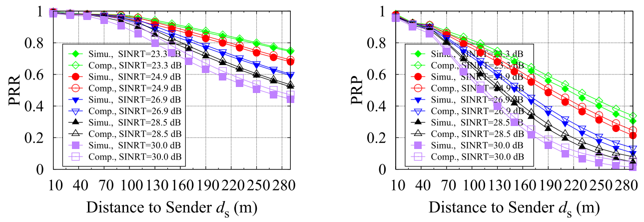

(a) (b)

Fig. 11. PRR, PRP comparisons between the theoretical model and the simulation in the 1-D scene. (a) PRR with the density of 0.132 vehicles/meter. (b) PRP with the density of 0.2 vehicles/meter.

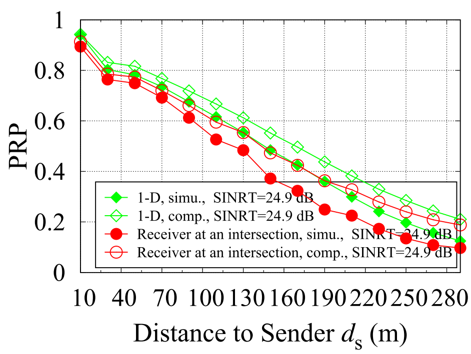

Fig. 12. PRP comparisons between the theoretical model and the simulation in 1-D, 2-D with the receiver at an intersection for the density of 0.5 vehicles/meter.

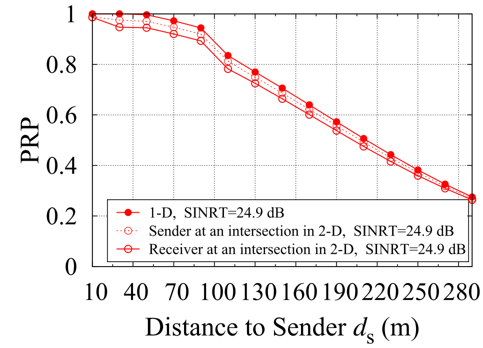

Fig. 13. PRP comparisons of 1-D scenario and two 2-D scenarios at the density of 0.066 vehicles/meter.

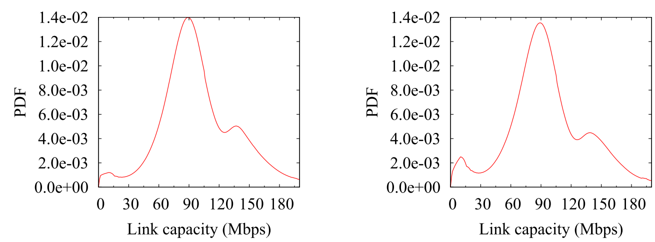

(a) (b)

Fig. 14. Link capacity of 1-D and 2-D with the density of 0.132 vehicles/meter. (a) 1-D. (b) 2-D with the receiver at an intersection.

decreasing trends. On the other hand, the larger the SINRTs, the stronger reception power and larger signal strength required to decode the received packet, and the vehicle nodes which are not satisfied with the receiving conditions will drop the packet causing the packet loss, thus the PRP decreasing trend with larger SINRT equaling 30.0 dB is more obvious than those of small values 28.5 dB, 26.9 dB, 24.9 dB and 23.3 dB. Fig. 11 gives PRR, PRP comparisons between the theoretical model and NS2 simulation in the 1-D with a density of 0.132 vehicles/meter, 0.132 vehicles/meter, respectively. The results show that the numerical computations of PRR are close to the simulations results, and the increases in d_{s} and SINRT also cause the PRR decreasing trends.

From Fig. 8–Fig. 11, we find that analytic results are more optimistic than simulation results, since the proposed analytic model assumptions consider the interference in $2r_{\mathrm{E}}$, while the random interferer for the receiver is regarded as the major interference if multiple interferers coexist in the shaded area, which may underestimate the interference calculations. On the other hand, as shown in Fig. 8–Fig. 11, the PRPs of theoretical model and NS2 simulation can fit well at the density of 0.066 for the 1-D scene and two 2-D intersection scenes. But, when the density equals 0.132 and 0.2, it is obvious that the discrepancies between the analytical model and simulation become large slightly compared with the low density case.

3) PRP of 1-D, 2-D With High Density: Fig. 12 presents the comparison results between the theoretical model and simulation with density equaling 0.5 vehicles/meter and SINRT equaling 24.9 dB for the 1-D, 2-D with the receiver at an intersection. It can be seen obviously the discrepancies become the largest compared with the density equaling 0.132 vehicles/meter and 0.2 vehicles/meter intermediate cases. The evaluations discrepancies for the analytical model mainly connect with whether the queueing system of semi-Markov based queueing model [8] could reach the steady-state. The queueing system will reach the saturated state with the increasing vehicle density, in our experiment with the vehicle density equaling 0.5, the discrepancies between the theoretical and simulation become large obviously.

C. Compare 1-D Scenario and Two 2-D Scenarios At an Intersection

We compare PRPs of 1-D scenario and two 2-D intersection scenarios with SINRT equaling 24.9 dB (315) as shown in Fig. 13. The performance of 1-D is the best since it suffers the least interference compared with two 2-D scenes. The dotted line represents PRPs of the situation where the sender is at an intersection, which is better than the scenario where the receiver is at an intersection. This is because the signals arriving at the intersection are interfered with the nodes in the four directions: up, down, left, and right. The farther the receiver is from the intersection, the less vertical interference will occur.

D. Link Capacity Analysis At 1-D and 2-D VANETs

Fig. 14 shows the PDF of the link capacity of the local VANET for BSM broadcast with different values of bandwidth at the 1-D and 2-D with the density of 0.132 vehicles/meter. It is

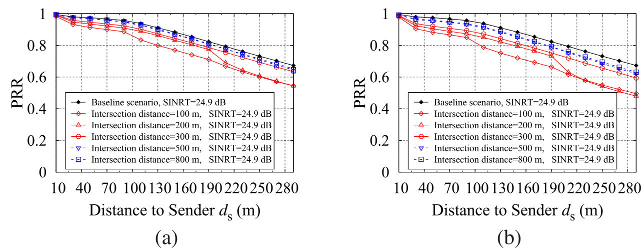

Fig. 15. PRR comparisons between multi-road with multi-intersection scenarios and the baseline at the density of 0.132 vehicles/meter. (a) Compare with three intersections.(b) Compare with nine intersections.

observed that PDF of the link capacity increases with the system bandwidth initially, but degrades when bandwidth (W) reaches 90 MHz or so. It is also observed that the probability of link capacity values equaling $[0, 30]$ in Fig. 14(b) is larger than that of Fig. 14(a). The above analyses also denote the mean of link capacity for 2-D is smaller than that of 1-D.

VI. Extension to Multi-Road With Multi-Intersection Scenarios

In this section, we discuss the effect on the PRR with the multiple intersections by simulation. We take the performance results of one intersection scenario by NS2 as the baseline, and the other two groups simulations of multi-road with multi-intersection scenes by NS2 as the comparisons. The first group is three equally spaced intersections where a horizontal road and three vertical roads intersections, and the second group is nine equally spaced intersections where three horizontal roads and three vertical roads intersections. Each group simulation corresponds to the distance between adjacent roads equaling 100 m, 200 m, 300 m, 400 m, 500 m, and 800 m, respectively. Each road extends 1 km outward in two directions except the road between the intersections. The communication range, the carrier sensing range, and the interference range are all 300 m. The density is set to 0.132 vehicles/meter, and SINRT is equal to 24.9 dB (315).

Fig. 15 shows the PRR comparisons between the baseline and the other scenarios that the distances between the intersections is larger or less than the carrier sensing range. We found that the closer the intersection, the worse the PRRs. When the intersection space is less than the sensing range of 300 m, there is a big gap with the baseline. Otherwise, when the intersection space is larger than the sensing range, the PRRs are almost the same as the baseline. The comparison results show that our model for analyzing 2-D intersection fits the scenario that the intersection space is larger than the sensing range.

VII. Conclusion

In this paper, we propose an analytic model based on SINR analysis for 1-D and 2-D VANETs, to evaluate the reliability and capacity of the IEEE 802.11 based broadcast wireless networks. The ordered statistics approach is utilized to reduce the computational complexity of the analytical models. Firstly, IEEE 802.11p modules regarding the SINR thresholds in NS2 are modified to adapt our SINR based analyses, and the mobility model enabled by SUMO incorporating the simulations not only enrich the simulation scenarios to evaluate the PRP but also account for the fact that evaluations for QoS metrics could utilize the static model in NS2 validations. Secondly, numerical results prove the effectiveness and the correctness of the proposed model: 1) The comparison results between the ordered and unordered model show that the proposed model with order statistic has greatly reduced the computational complexity. 2) The simulation results further validate the numerical results, and the comparison discrepancies at high density become the largest. The PDF, CDF for 1-D and 2-D are obtained by numerical solutions and then the QoS metrics PRR, PRP, and link capacity are obtained. Thirdly, the comparisons between the 2-D intersection with two types of geometry locations and 1-D highway, show that 2-D intersection geometry location with the receiver at the intersection has the lowest performance values, including the PRP and PRR. Finally, our model for analyzing 2-D intersection is fit to the multiple intersections that the intersection space is larger than the carrier sensing range.

Appendix A
Derivation of $f_{D_{I_3}|(x_0,x_r)}(y)$

Let's look at PDF of I_3. Denote $d_{i_3}(i_3 = 1,\ldots,l'')$ be the distance between the origin and the i_3-th node within the up shaded region. Given NHPP distribution of the distance between nodes, independent random variables S_{i_3} ($\sqrt{{r_{\mathrm{E}}}^2 - {x_0}^2} \le S_{i_3} \le \sqrt{4{r_{\mathrm{E}}}^2 - {x_0}^2}$) denote unordered distances between the origin and the nodes in the up shaded region in vertical axis. Let the number of vehicles in the interval $[\sqrt{{r_{\mathrm{E}}}^2 - {x_0}^2}, r]$ and $[\sqrt{{r_{\mathrm{E}}}^2 - {x_0}^2}, \sqrt{4{r_{\mathrm{E}}}^2 - {x_0}^2}]$ be denoted by $N(r), N(s)$, respectively. The CDF of S_{i_3} is given by Theorem 6.2 in [40]:

$$\begin{aligned}F_{S_{i_3}}(r) &= P(S_{i_1} \le r | N(s) = 1)\\ &= \frac{P[N(r) = 1, N(s) - N(r) = 0]}{P[N(s) = 1]}\\ &= \frac{\int_{\sqrt{r_{\mathrm{E}}^2 - x_0^2}}^{r} \beta(z)\mathrm{d}z}{\int_{\sqrt{r_{\mathrm{E}}^2 - x_0^2}}^{\sqrt{4r_{\mathrm{E}}^2 - x_0^2}} \beta(z)\mathrm{d}z},\end{aligned}$$

The PDF of S_{i_3} is

$$f_{S_{i_3}}(r) = \frac{\beta(r)}{\int_{\sqrt{r_{\mathrm{E}}^2 - x_0^2}}^{\sqrt{4r_{\mathrm{E}}^2 - x_0^2}} \beta(z)\mathrm{d}z}. \tag{41}$$

Given $D_{\mathrm{S}} = |x_{\mathrm{r}} - x_0|$ is the distance between T and R, the distance between interference node and node R is denoted as $D_{I_3} = \sqrt{d_{i_3}^2 + x_{\mathrm{r}}^2}$ ($\sqrt{r_{\mathrm{E}}^2 + x_r^2 - x_0^2} \le D_{I_3} \le \sqrt{4r_{\mathrm{E}}^2 + x_r^2 - x_0^2}$). We have:

$$\begin{aligned}F_{D_{I_3}|(x_0,x_{\mathrm{r}},i_3)}(y) &= P(D_{I_3} \le y)\\ &= P(d_{i_3}^2 + x_{\mathrm{r}}^2 \le y^2)\\ &= P(d_{i_3} \le \sqrt{y^2 - x_{\mathrm{r}}^2})\\ &= F_{d_{i_3}}(\sqrt{y^2 - x_{\mathrm{r}}^2}), i_3 = 1,\ldots,l''.\end{aligned} \tag{42}$$

The PDF of the D_{I_3} is obtained as

$$f_{D_{I_3}|(x_0,x_{\rm r},i_3)}(x) = \frac{{\rm d}F_{D_{I_3}|(x_0,x_{\rm r},i_3)}(x)}{{\rm d}x}.$$

The probability that there are l'' nodes in the up shaded area is:

$$P\left[l,''\left(\sqrt{r_{\rm E}^2-x_0^2},\sqrt{4r_{\rm E}^2-x_0^2}\right)\right] = \frac{\left(\int_{\sqrt{r_{\rm E}^2-x_0^2}}^{\sqrt{4r_{\rm E}^2-x_0^2}}\beta(y){\rm d}y\right)^{l''}\exp\left(-\int_{\sqrt{r_{\rm E}^2-x_0^2}}^{\sqrt{4r_{\rm E}^2-x_0^2}}\beta(y){\rm d}y\right)}{l''!}.$$

Then, the total D_{I_3}'s conditional PDF can be expressed as

$$f_{D_{I_3}|(x_0,x_{\rm r})}(y) = \sum_{l''=1}^{\infty} P\left[l,''\left(\sqrt{r_{\rm E}^2-x_0^2},\sqrt{4r_{\rm E}^2-x_0^2}\right)\right] \times \sum_{i_3=1}^{l''} f_{D_{I_3}|(x_0,x_{\rm r},i_3)}(y)p_{i_3}. \tag{43}$$

where p_{i_3} is the probability that the interference I_3 is the i_3-th node within the right shaded region, which is evaluated as $p_{i_3} = 1/l''$. Substituting p_{i_3} into (43) can obtain

$$f_{D_{I_3}|(x_0,x_{\rm r})}(y) = \frac{\beta(\sqrt{y^2-x_r^2})}{\int_{\sqrt{r_{\rm E}^2-x_0^2}}^{\sqrt{4r_{\rm E}^2-x_0^2}}\beta(z){\rm d}z}. \tag{44}$$

APPENDIX B
THE INTERFERENCE DISTANCE DISTRIBUTION OF CASE 2 R IN $(0, y_{\rm r})$

Denote $d_{i_1}(i_1 = 1,\ldots,l)$ be the distance between the tagged node T and the i_1-th node within the right shaded region. Given NHPP distribution of distance between nodes, and independent random variables $r_{\rm E} \le S_{i_1} \le 2r_{\rm E}(i_1 = 1,\ldots,l)$ denote the unordered distances between the tagged node T and the nodes in the right shaded region, the CDF of S_{i_1} is given by Theorem 6.2 in [40] as

$$\begin{aligned} F_{S_{i_1}}(r) &= P(S_{i_1} \le r|N(s)=1) \\ &= \frac{P[N(r)=1, N(s)-N(r)=0]}{P[N(s)=1]} \\ &= \frac{\int_{r_{\rm E}+x_0}^{r+x_0}\beta(z)dz}{\int_{r_{\rm E}+x_0}^{2r_{\rm E}+x_0}\beta(z)dz}, \\ & r_{\rm E} \le r \le 2r_{\rm E}, i_1 = 1,\ldots,l. \end{aligned}$$

The PDF of S_{i_1} is

$$f_{S_{i_1}}(r) = \frac{\beta(r+x_0)}{\int_{r_{\rm E}+x_0}^{2r_{\rm E}+x_0}\beta(z){\rm d}z}.$$

Then, according to Theorem 6.2 in [40], $d_{i_1}(i_1 = 1,\ldots,l)$ are the order statistics of the random variables $S_{i_1}(i_1 = 1,\ldots,l)$. Thus, the CDF and PDF of distance d_{i_1} $(r_{\rm E} \le d_{i_1} \le 2r_{\rm E})$ can be calculated as

$$F_{d_{i_1}}(\tau) = P(d_{i_1} \le \tau) = \sum_{j=i_1}^{l}\binom{l}{j}F_{S_{i_1}}{}^{j}(\tau)\left[1-F_{S_{i_1}}(\tau)\right]^{l-j},$$

$$f_{d_{i_1}}(\tau) = \frac{{\rm d}F_{d_{i_1}}(\tau)}{{\rm d}\tau}, r_{\rm E} \le \tau \le 2r_{\rm E}, i_1 = 1,\ldots,l.$$

Similarly, independent random variables $S_{i_3}(\sqrt{r_{\rm E}^2-x_0^2} \le S_{i_3} \le \sqrt{4r_{\rm E}^2-x_0^2})$ denote unordered distance between the origin and the nodes in the up shaded region in vertical axis. The CDF and PDF of S_{i_3} and be calculated as

$$F_{S_{i_3}}(r) = \frac{\int_{\sqrt{r_{\rm E}^2-x_0^2}}^{r}\beta(z){\rm d}z}{\int_{\sqrt{r_{\rm E}^2-x_0^2}}^{\sqrt{4r_{\rm E}^2-x_0^2}}\beta(z){\rm d}z}, f_{S_{i_3}}(r) = \frac{\beta(r)}{\int_{\sqrt{r_{\rm E}^2-x_0^2}}^{\sqrt{4r_{\rm E}^2-x_0^2}}\beta(z){\rm d}z},$$

$$\sqrt{r_{\rm E}^2-x_0^2} \le r \le \sqrt{4r_{\rm E}^2-x_0^2}.$$

The $d_{i_3}(i_3 = 1,\ldots,l'')$ are the order statistics of the random variables S_{i_3}. The CDF and PDF of distance d_{i_3} $(\sqrt{r_{\rm E}^2-x_0^2} \le d_{i_3} \le \sqrt{2r_{\rm E}^2-x_0^2})$ can be calculated as

$$F_{d_{i_3}}(\tau) = P(d_{i_3} \le \tau) = \sum_{j=i_3}^{l''}\binom{l''}{j}F_{S_{i_3}}^{j}(\tau)(1-F_{S_{i_3}}(\tau))^{l''-j},$$

$$f_{d_{i_3}}(\tau) = \frac{{\rm d}F_{d_{i_3}}(\tau)}{{\rm d}\tau}, i_3 = 1,\ldots,l''.$$

Given $D_{\rm S} = ({y_{\rm r}}^2 + {x_0}^2)^{1/2}$ is the distance between T and R, the distance between interference node and node R is denoted as $D_{I_1}(\sqrt{(r_{\rm E}+x_0)^2+y_r^2} \le D_{I_1} \le \sqrt{(2r_{\rm E}+x_0)^2+y_r^2})$ and $D_{I_3}(\sqrt{r_{\rm E}^2-x_0^2}-y_{\rm r} \le D_{I_3} \le \sqrt{4r_{\rm E}^2-x_0^2}-y_{\rm r})$, respectively. We have:

$$\begin{aligned} F_{D_{I_1}|(x_0,y_{\rm r},i_1)}(x) &= P(D_{I_1} \le x) \\ &= P(d_{i_1} \le \sqrt{x^2-y_r^2}-x_0) \\ &= F_{d_{i_1}}(\sqrt{x^2-y_r^2}-x_0), i_1 = 1,\ldots,l, \\ F_{D_{I_3}|(x_0,y_{\rm r},i_3)}(y) &= P(D_{I_3} \le y) \\ &= P(d_{i_3} \le y+y_{\rm r}) \\ &= F_{d_{i_3}}(y+y_{\rm r}), i_3 = 1,\ldots,l''. \end{aligned}$$

The PDFs of the distances are obtained as

$$f_{D_{I_1}|(x_0,y_{\rm r},i_1)}(x) = \frac{{\rm d}F_{D_{I_1}|(x_0,y_{\rm r},i_1)}(x)}{{\rm d}x},$$

$$f_{D_{I_3}|(x_0,y_{\rm r},i_3)}(y) = \frac{{\rm d}F_{D_{I_3}|(x_0,y_{\rm r},i_3)}(y)}{{\rm d}y}.$$

The probability that there are $l(l'')$ nodes in the right(up) shaded area is

$$P[l,(r_{\rm E}+x_0, 2r_{\rm E}+x_0)] = \frac{\left(\int_{r_{\rm E}+x_0}^{2r_{\rm E}+x_0}\beta(x){\rm d}x\right)^{l}\exp\left(-\int_{r_{\rm E}+x_0}^{2r_{\rm E}+x_0}\beta(x){\rm d}x\right)}{l!},$$

$$P\left[l,''\left(\sqrt{r_{\mathrm{E}}^{2}-x_{0}^{2}},\sqrt{4r_{\mathrm{E}}^{2}-x_{0}^{2}}\right)\right] = \frac{\left(\int_{\sqrt{r_{\mathrm{E}}^{2}-x_{0}^{2}}}^{\sqrt{4r_{\mathrm{E}}^{2}-x_{0}^{2}}}\beta(y)\mathrm{d}y\right)^{l''}\exp\left(-\int_{\sqrt{r_{\mathrm{E}}^{2}-x_{0}^{2}}}^{\sqrt{4r_{\mathrm{E}}^{2}-x_{0}^{2}}}\beta(y)\mathrm{d}y\right)}{l''!}.$$

Then, the total D'_{I_1}s and D'_{I_3}s conditional PDF can be expressed as

$$f_{D_{I_1}|(x_0,y_{\mathrm{r}})}(x) = \sum_{l=1}^{\infty} P(l,(r_{\mathrm{E}}+x_0, 2r_{\mathrm{E}}+x_0)) \times \sum_{i_1=1}^{l} f_{D_{I_1}|(x_0,y_{\mathrm{r}},i_1)}(x)p_{i_1}, \tag{45}$$

$$f_{D_{I_3}|(x_0,y_{\mathrm{r}})}(y) = \sum_{l''=1}^{\infty} P[l,''(\sqrt{r_{\mathrm{E}}^{2}-x_{0}^{2}},\sqrt{4r_{\mathrm{E}}^{2}-x_{0}^{2}})] \times \sum_{i_3=1}^{l''} f_{D_{I_3}|(x_0,y_{\mathrm{r}},i_3)}(y)p_{i_3}. \tag{46}$$

where $p_{i_1}(p_{i_3})$ is the probability that the interference $I_1(I_3)$ is the $i_1(i_3)$-th node within the right (up) shaded region, which is evaluated as $p_{i_1}=1/l(i_1=1,\ldots,l)$, $p_{i_3}=1/l''(i_3=1,\ldots,l'')$. So, (45) and (46) become the following forms:

$$\begin{aligned} f_{D_{I_1}|(x_0,y_{\mathrm{r}})}(x) &= f_{S_{i_1}}(\sqrt{x^2-y_{\mathrm{r}}^2}) = \frac{\beta(\sqrt{x^2-y_{\mathrm{r}}^2})}{\int_{r_{\mathrm{E}}+x_0}^{2r_{\mathrm{E}}+x_0}\beta(z)\mathrm{d}z}, \\ f_{D_{I_3}|(x_0,y_{\mathrm{r}})}(y) &= f_{S_{i_3}}(y+y_{\mathrm{r}}) = \frac{\beta(y+y_{\mathrm{r}})}{\int_{\sqrt{r_{\mathrm{E}}^{2}-x_{0}^{2}}}^{\sqrt{4r_{\mathrm{E}}^{2}-x_{0}^{2}}}\beta(z)\mathrm{d}z}. \end{aligned} \tag{47}$$

The derivation methods of PDF of D_{I_2} and D_{I_4} are similar to those of D_{I_1} and D_{I_3}.

REFERENCES

[1] *Dedicated Short Range Communications (DSRC) Message Set Dictionary*, SAE Std. J2735, SAE Int., DSRC Committee, Mar. 2016.

[2] J. B. Kenney, "Dedicated short-range communications (DSRC) standards in the united states," *Proc. IEEE*, vol. 99, no. 7, pp. 1162–1182, Jul. 2011.

[3] O. Andrisano, R. Verdone, and M. Nakagawa, "Intelligent transportation systems: The role of third generation mobile radio networks," *IEEE Commun. Mag.*, vol. 38, no. 9, pp. 144–151, Sep. 2000.

[4] M. Torrent-Moreno, D. Jiang, and H. Hartenstein, "Broadcast reception rates and effects of priority access in 802.11-based vehicular ad-hoc networks," in *Proc. ACM Int. Workshop VANET*, PA, USA, 2004, pp. 10–18.

[5] *Intelligent Transport Systems (ITS); Vehicular Communications; Basic Set of Applications; Part 2: Specification of Cooperative Awareness Basic Service*, European Std. ETSI EN 302 637-2, V1.3.2, Nov. 2014.

[6] K. Zheng, Q. Zheng, P. Chatzimisios, W. Xiang, and Y. Zhou, "Heterogeneous vehicular networking: A. survey on architecture, challenges, and solutions," *IEEE Commun. Surveys Tuts.*, vol. 17, no. 4, pp. 2377–2396, Jun. 2015.

[7] Vehicle Safety Communications Project: Task 3 Final Report: Identify Intelligent Vehicle Safety Applications Enabled by DSRC, U.S. Dept. Trans., Nat. Highway Traffic Safety Admin., Rep. DOT HS 809 859, Mar. 2005.

[8] X. Yin, X. Ma, and K. S. Trivedi, "An interacting stochastic models approach for the performance evaluation of DSRC vehicular safety communication," *IEEE Trans. Comput.*, vol. 62, no. 5, pp. 873–885, May 2013.

[9] Y. Yao, L. Rao, and X. Liu, "Performance and reliability analysis of IEEE 802.11p safety communication in a highway environment," *IEEE Trans. Veh. Technol.*, vol. 62, no. 9, pp. 4198–4212, Nov. 2013.

[10] Z. Tong, H. Lu, M. Haenggi, and C. Poellabauer, "A stochastic geometry approach to the modeling of DSRC for vehicular safety communication," *IEEE Trans. Intell. Transport. Syst.*, vol. 17, no. 5, pp. 1448–1458, May 2016.

[11] W. Yanbin, W. Zhuofei, Z. Jing, L. Zhijuan, and M. Xiaomin, "Analysis and adaptive optimization of vehicular safety message communications at intersections," *Ad Hoc Netw.*, vol. 107, Oct. 2020, Art. no. 102241.

[12] J. P. Jeyaraj and M. Haenggi, "Reliability analysis of V2V communications on orthogonal street systems," in *Proc. IEEE GLOBECOM IEEE Glob. Commun. Conf.*, Singapore, Dec. 2017, pp. 1–6.

[13] B. E. Y. Belmekki, A. Hamza, and B. Escrig, "On the outage probability of vehicular communications at intersections over nakagami-m fading channels," in *Proc. IEEE 91st Veh. Technol. Conf. (VTC Spring)*, Antwerp, Belgium, Belgium, May 2020, pp. 1–5.

[14] E. Steinmetz, M. Wildemeersch, T. Q. S. Quek, and H. Wymeersch, "A stochastic geometry model for vehicular communication near intersections," in *Proc. IEEE GLOBECOM Workshops*, Dec. 2015, pp. 1–6.

[15] T. V. Nguyen, F. Baccelli, K. Zhu, and S. S. X. Z. Wu, "A performance analysis of csma based broadcast protocol in vanets," in *Proc. 32th IEEE INFOCOM*, Turin, Italy, Apr. 2013, pp. 2805–2813.

[16] M. Ni, J. Pan, L. Cai, J. Yu, H. Wu, and Z. Zhong, "Interference-based capacity analysis for vehicular ad hoc networks," *IEEE Commun. Lett.*, vol. 19, no. 4, pp. 621–624, Apr. 2015.

[17] X. Ma, H. Lu, J. Zhao, Y. Wang, J. Li, and M. Ni, "Comments on "interference-based capacity analysis of vehicular ad hoc networks," *IEEE Commun. Lett.*, vol. 21, no. 10, pp. 2322–2325, Oct. 2017.

[18] P. A. Lopez *et al.*, "Microscopic traffic simulation using sumo," in *Proc. 21st Int. Conf. Intell. Transport. Syst.*, Maui, HI, USA, Nov. 2018, pp. 2575–2582.

[19] M. van Eenennaam, W. K. Wolterink, G. Karagiannis, and G. Heijenk, "Exploring the solution space of beaconing in vanets," in *Proc. IEEE VNC*, Tokyo, Japan, Oct. 2009, pp. 1–8.

[20] M. I. Hassan, H. L. Vu, and T. Sakurai, "Performance analysis of the IEEE 802.11 MAC protocol for DSRC safety applications," *IEEE Trans. Veh. Technol.*, vol. 60, no. 8, pp. 3882–3896, Oct. 2011.

[21] K. A. Hafeez, L. Zhao, B. Ma, and J. W. Mark, "Performance analysis and enhancement of the DSRC for VANET's safety applications," *IEEE Trans. Veh. Technol.*, vol. 62, no. 7, pp. 3069–3083, Sep. 2013.

[22] X. Ma, X. Yin, M. Wilson, and K. S. Trivedi, "Mac and application-level broadcast reliability in vanets with channel fading," in *Proc. Int. Conf. Comput., Netw. Commun.*, San Diego, CA, USA, Jan. 2013, pp. 756–761.

[23] X. Ma, M. Wilson, X. Yin, and K. S. Trivedi, "Performance of vanet safety message broadcast at rural intersections," in *Proc. 9th Int. Wirel. Commun. Mobile Comput. Conf.*, Jul. 2013, pp. 1617–1622.

[24] X. Ma, G. Butron, and K. Trivedi, "Modeling of vanet for bsm safety messaging at intersections with non-homogeneous node distribution," in *Proc. Int. Workshop Commun. Technol. Veh.*, San Sebastián, Spain, May 2016, pp. 149–162.

[25] M. Haenggi and R. K. Ganti, "Interference in large wireless networks," *Found. Trends Netw.*, vol. 3, no. 2, pp. 127–248, Feb. 2009.

[26] H. Q. Nguyen, F. Baccelli, and D. Kofman, "A stochastic geometry analysis of dense IEEE 802.11 networks," in *Proc. 26th IEEE INFOCOM 26th IEEE Int. Conf. Comput. Commun.*, Barcelona, Spain, May 2007, pp. 1199–1207.

[27] T. Kimura, H. Saito, and H. Honda, "Optimal transmission range for V2I communications on congested highways," in *Proc. IEEE Annu. Int. Symp. Pers., Indoor, Mobile Radio Commun.*, Montreal, QC, Canada, Oct. 2017, pp. 1–7.

[28] T. Kimura, H. Saito, H. Honda, and R. Kawahara, "Modeling urban its communication via stochastic geometry approach," in *Proc. IEEE 84th Veh. Technol. Conf.*, Montreal, QC, Canada, Sep. 2016, pp. 1–5.

[29] M. Ni, M. Hu, Z. Wang, and Z. Zhong, "Packet reception probability of vanets in urban intersecton scenario," in *Proc. Int. Conf. Connected Veh. Expo*, Shenzhen, China, Oct. 2015, pp. 124–125.

[30] M. Abdulla, E. Steinmetz, and H. Wymeersch, "Vehicle-to-vehicle communications with urban intersection path loss models," in *Proc. IEEE GLOBECOM Workshops*, Washington, DC, USA, Dec. 2016, pp. 1–6.

[31] C. Choi and F. Baccelli, "An analytical framework for coverage in cellular networks leveraging vehicles," *IEEE Trans. Commun.*, vol. 66, no. 10, pp. 4950–4964, Oct. 2018.

[32] V. V. Chetlur and H. S. Dhillon, "Coverage and rate analysis of downlink cellular vehicle-to-everything (c-v2x) communication," *IEEE Trans. Wirel. Commun.*, vol. 19, no. 3, pp. 1738–1753, Mar. 2020.

[33] M. N. Sial, Y. Deng, J. Ahmed, A. Nallanathan, and M. Dohler, "Stochastic geometry modeling of cellular v2x communication over shared channels," *IEEE Trans. Veh. Technol.*, vol. 68, no. 12, pp. 11 873–11 887, Oct. 2019.

[34] J. Zhao, Z. Li, Y. Wang, Z. Wu, X. Ma, and Y. Zhao, "An analytical framework for reliability evaluation of d-dimensional IEEE 802.11 broadcast wireless networks," *Wirel. Netw.*, vol. 26, pp. 3373–3394, Feb. 2020.

[35] T. Yang, G. Mao, and W. Zhang, "Connectivity of large-scale csma networks," *IEEE Trans. Wirel. Commun.*, vol. 11, no. 6, pp. 2266–2275, Jun. 2012.

[36] J. Zhao, Z. Wu, Y. Wang, and X. Ma, "Adaptive optimization of qos constraint transmission capacity of vanet," *Veh. Commun.*, vol. 17, pp. 1–9, Jun. 2019.

[37] Q. Chen, F. Schmidt-Eisenlohr, D. Jiang, M. Torrent-Moreno, L. Delgrossi, and H. Hartenstein, "Overhaul of IEEE 802.11 modeling and simulation in ns-2," in *Proc. 10th ACM Symp. Model., Anal., Simul. Wirel. Mobile Syst.*, NY, USA, Oct. 2007, pp. 159–168.

[38] J. Li, Y. Zhang, Z. Jing, X. Ma, and Y. Wang, "NS-2 simulation of VANET for safety applications: Issues and solutions," in *Proc. 8th Int. Conf. Comput. Model. Simul.*, Canberra Australia, Jan. 2017, pp. 67–72.

[39] W. Gropp, E. Lusk, N. Doss, and A. Skjellum, "A high-performance, portable implementation of the MPI message passing interface standard," *Parallel. Comput.*, vol. 22, no. 6, pp. 789–828, Sep. 1996.

[40] K. S. Trivedi, *Probability & Statistics With Reliability, Queuing and Computer Science Applications*. Hoboken, NJ, USA: John Wiley & Sons, 2008.

[41] F. Bai, T. Elbatt, G. Hollan, H. Krishnan, and V. Sadekar, "Towards characterizing and classifying communication-based automotive applications from a wireless networking perspective," in *Proc. IEEE Workshop Automot. Netw. Appl.*, San Francisco, CA, USA, 2006, pp. 1–25.

Jing Zhao (Member, IEEE) received the Ph.D. degree in computer science and technology from the Harbin Institute of Technology, Harbin, China, in 2006. In 2010, she was with the Department of Electrical and Computer Engineering, Duke University, Durham, NC, USA, as a Postdoctoral Researcher under supervision of Dr. Kishor Trivedi. From 2006 to 2018, she was a Professor with the School of Computer Science and Technology, Harbin Engineering University, Harbin, China. She is currently a Professor with the School of Software Technology, Dalian University of Technology, Dalian, China. Her research interests include physical layer and MAC layer of vehicular ad hoc networks, reliability engineering, and network optimization.

Yanbin Wang received the Ph.D. degree from Industrial Engineering Department, the Harbin Institute of Technology, Harbin, China, in 2006. In 2010, he was a Research Associate with the Department of Electrical and Computer Engineering, Duke University, Durham, NC, USA. He is currently an Associate Professor with Industrial Engineering Department, the Harbin Institute of Technology, Harbin, China. His research interests include vehicular ad hoc networks, quality management, scheduling, and optimization.

Hualin Lu received the M.S. degree from the School of Computer Science and Technology, Harbin Engineering University, Harbin, China, in 2017. From 2018 to 2019, he was a Container Software Engineer with Xiaomi Company Ltd., Beijing, China. He is currently a Software Engineer with Bilibili Company Ltd., Shanghai, China. His research interests include container cloud system, software testing, DevOps, and IoT security.

Zhijuan Li received the M.S. degree in 2013 with the School of Computer Science and Technology, Harbin Engineering University, Harbin, China, where she is currently working toward the Ph.D. degree. From 2013 to 2016, she was a Software Engineer with Harbin Yuguang Virtual Network Technology Company, Ltd, Harbin, China. Her research interests include vehicular ad hoc network and fog computing.

Xiaomin Ma Senior Member, IEEE) received the B.E. and M.E. degrees in electrical engineering, and the Ph.D. degree in information engineering from the Beijing University of Posts and Telecommunications, Beijing, China, in 1984, 1989, and 1999. From 2000 to 2002, he was a Postdoctoral Fellow with the Department of Electrical and Computer Engineering, Duke University, Durham, NC, USA. He is currently a Professor with the Department of Engineering, Oral Roberts University, Tulsa, OK, USA. His research interests include stochastic modeling and analysis of computer and communication systems, physical layer and MAC layer of vehicular ad hoc wireless networks, computational intelligence and its applications to coding, signal processing, and control, and quality of service and call admission control protocols in wireless networks.